NASA TECHNICAL NOTE

NASA TN D-5970

AN INTEGRAL ANALYSIS OF HEAT TRANSFER DOWNSTREAM OF A REARWARD-FACING STEP WITH SMALL COOLANT INJECTION

by Keiichi Karashima

Langley Research Center
Hampton, Va. 23365

NATIONAL AERONAUTICS AND SPACE ADMINISTRATION • WASHINGTON, D. C. • DECEMBER 1970

1. Report No.	2. Government Accession No.	3. Recipient's Catalog No.
NASA TN D-5970		

4. Title and Subtitle	5. Report Date
AN INTEGRAL ANALYSIS OF HEAT TRANSFER DOWNSTREAM OF A REARWARD-FACING STEP WITH SMALL COOLANT INJECTION	December 1970
	6. Performing Organization Code
7. Author(s)	8. Performing Organization Report No.
Keiichi Karashima	L-6689
	10. Work Unit No.
9. Performing Organization Name and Address	124-64-03-02
NASA Langley Research Center Hampton, Va. 23365	11. Contract or Grant No.
	13. Type of Report and Period Covered
12. Sponsoring Agency Name and Address	Technical Note
National Aeronautics and Space Administration Washington, D.C. 20546	14. Sponsoring Agency Code

15. Supplementary Notes

This research was accomplished while the author held a National Research Council Postdoctoral Resident Research Associateship at NASA Langley Research Center. Author is now at University of Tokyo, Tokyo, Japan.

16. Abstract

Slot cooling is analyzed theoretically for the case where the approaching boundary layer is thin, relative to the slot height, and the coolant flow rate is small. The analysis treats the turbulent mixing layer, the recompression region, and the turbulent boundary layer downstream of the slot. The analysis shows that coolant injection reduces total heating downstream of the slot whereas local heating in the jet-mixing and recompression regions may increase.

17. Key Words (Suggested by Author(s))	18. Distribution Statement
Mass transfer cooling Slot cooling Heat transfer	Unclassified – Unlimited

19. Security Classif. (of this report)	20. Security Classif. (of this page)	21. No. of Pages	22. Price*
Unclassified	Unclassified	82	$3.00

*For sale by the Clearinghouse for Federal Scientific and Technical Information Springfield, Virginia 22151

AN INTEGRAL ANALYSIS OF HEAT TRANSFER DOWNSTREAM OF A REARWARD-FACING STEP WITH SMALL COOLANT INJECTION

By Keiichi Karashima[1]
Langley Research Center

SUMMARY

This paper presents an approximate analysis of heat transfer downstream of a two-dimensional rearward-facing step followed by an infinite flat plate placed in a uniform supersonic stream. It is assumed that the thickness of the oncoming boundary layer is small compared with the step height and, that the coolant mass is injected into the dead-air region through the step face at a small flow rate. The whole flow field is divided into three regions: a jet mixing region, a recompression region, and a fully developed turbulent boundary layer.

It is shown that if there is no coolant flow, the flow separation accompanying a rearward-facing step and the associated recompression provide rather high heating rates in these regions when compared with the corresponding flat-plate flow. In the range of a very low coolant flow rate, although local heating rate in these high heating regions decreases, net heat transfer to the wall in these regions increases slightly because of their elongation.

On the other hand, a large amount of mass transport due to turbulent mixing is shown to result in considerable heat-transfer reduction because of growth of the boundary-layer thickness in the region downstream of recompression; thus, a favorable compensation for the increased heating encountered upstream is indicated.

It is shown that the overall effectiveness of coolant injection becomes a maximum at a very low coolant flow rate, and higher effectiveness can be obtained for smaller thicknesses of oncoming boundary layer; thus, an upstream location of the coolant slot is preferable. Moreover, examination of effect of coolant slot height reveals that if thickness of the oncoming boundary layer is fixed, there exists an optimum coolant slot height for which overall effectiveness of film cooling is a maximum.

---

[1]NRC-NASA Resident Research Associate, now at University of Tokyo, Tokyo, Japan.

INTRODUCTION

Film cooling is used to alleviate severe aerodynamic heating which is encountered in many types of engineering problems with high-enthalpy gas flow. It is used, for instance, to cool walls of combustion chambers and nozzles in jet engines and rocket motors, blades in gas-turbine engines, and nozzle walls of high-enthalpy wind tunnels. For entry from earth orbit, film cooling may have the capability of replacing conventional ablative heat shields.

A number of studies have been conducted on the film-cooling problem, mainly by experimental methods, over a long period of time; therefore, considerable information is available about the correlation between film cooling effectiveness and coolant flow rate. (See refs. 1 to 5.) The effect of coolant flow rate on adiabatic wall temperature has been established empirically for the case of incompressible boundary-layer flow over a heated surface, and analyses for this case are presented in references 6 and 7, for example.

The present approach to the problem is to treat the case of the heat transfer rate downstream of a rearward-facing slot where coolant is injected tangential to the surface. The wall is maintained at an isothermal condition, for example, by first vaporizing the fluid on the inside of the vehicle wall, a condition of interest for some entry vehicles. No theoretical approach has been developed for solving this problem. The problem is complex, because the concentrated injection at a given location produces an abrupt change of boundary layer characteristics, and this in turn causes a complicated interaction between the internal dissipative flow and the external isentropic supersonic flow. Moreover, if the internal dissipative flow is turbulent, even theoretical knowledge of the effect of compressibility on the flow is meager.

The purpose of the present paper is to demonstrate the importance of turbulent mixing in determining the characteristics of dissipative flow downstream of the point of coolant mass injection and to formulate this concept in quantitative terms to clarify the effect of various aerodynamic parameters. The resulting equations are solved numerically for the isothermal wall condition, and the solutions are examined in terms of the gross heat transfer characteristics downstream of the slot.

To formulate and solve the problem, several assumptions are introduced which limit the applicability of the results. First, based on the experimental results of reference 4, the problem is related to that associated with the base pressure behind a two-dimensional rearward-facing step through which mass is injected into the dead-air region, so that the configuration analyzed is a rearward facing two-dimensional step

followed by an infinite flat plate. Further, the oncoming boundary layer thickness is assumed to be small compared with the step height. Also, the coolant flow rate is assumed to be small, so that the velocity in the dead-air region can be neglected. Other assumptions, which do not reduce the scope of the problem being solved, are introduced in the theoretical development as required.

SYMBOLS

a	speed of sound
C	length of plate lip
C_f	skin-friction coefficient
$C_{H,\infty}$	energy transfer coefficient defined by equation (87)
C_n	constant of integration
C_q	heat-transfer coefficient
c_1	constant of proportionality
c_p	specific heat at constant pressure
D	height of step
e	internal energy
F,G	functions defined by equations (16b) and (16c)
F_1,F_2	functions of κ defined by equations (68)
f	function
H	stagnation enthalpy
h	static enthalpy

I	momentum flux defined by equation (47)
J	energy flux
K	*mixing coefficient*
K_D, K_M	constants of proportionality with respect to boundary-layer thickness
L	length of separated region
l	width of recompression region
M	Mach number
$\dot{M}$	coolant flow rate defined by equation (33)
m	reduced mass flux defined by equations (58)
$\tilde{m}$	mass flux defined by equation (46)
$\overline{m}$	nondimensional mass flux defined by equations (74)
$N_{Pr,t}$	turbulent Prandtl number
N_{Re}	Reynolds number, $u_\infty C/\nu_\infty$
$N_{Re,D}$	Reynolds number, $u_\infty D/\nu_\infty$
$N_{Re,L}$	Reynolds number, $u_1 L/\nu_1$
$N_{Re,\infty}$	Reynolds number, $u_\infty x/\nu_\infty$
P	function of κ and w_e defined by equation (62)
p	pressure
Q	heat input defined by equations (35)
q	heat-transfer rate

$\tilde{q}$ mean heat-transfer rate

$\tilde{q}_w$ heat-transfer rate on a flat plate (Van Driest's solution)

R gas constant

S surface of control volume

T temperature

$\tilde{T}$ mean temperature across viscous layer in recompression region

u,v velocity components

$\tilde{u}$ mean velocity defined by equation (49)

V resultant velocity

W_p work done on gas by pressure, defined by equations (35)

W_s work done on gas by shear, defined by equations (35)

w reduced velocity defined by equations (58)

X constant of proportionality pertinent to scale factor

x,y coordinates

$\bar{x}$ nondimensional distance defined by equations (74)

y_m mean thickness of mixing layer

Z parameter defined by $\dfrac{C}{D\sqrt[n]{R_e}}$

α,β constants defined by equations (90)

γ ratio of specific heats

δ	thickness of boundary layer
δ^*	displacement thickness
$\bar{\delta}$	nondimensional thickness of boundary layer defined by equations (74)
ϵ	angle between external flow direction and X-axis in jet mixing region
ζ	similarity variable defined by equation (8)
η_f	local effectiveness of coolant injection in region of fully developed turbulent boundary layer
η_T	overall effectiveness of coolant injection
θ	flow deflection angle of external stream
θ^*	momentum thickness
κ	parameter defined by equation (50)
λ	wall enthalpy ratio defined by H_w/H_∞
μ	viscosity
ν	kinematic viscosity
ξ,η	coordinates in corresponding incompressible flow
ρ	density
$\tilde{\rho}$	mean density across viscous layer in recompression region
σ	scale factor
τ	shearing stress
ϕ	parameter defined by equation (64)

ψ stream function

ω power index for viscosity-temperature law

Subscripts:

o stagnation condition of oncoming flow or conditions without coolant flow

1 external flow conditions in jet mixing region

2 flow conditions at point of injection

b conditions at base of step without coolant flow

c conditions of coolant flow at slot exit

d conditions on dividing stream line

e external stream conditions in recompression region

i conditions in corresponding incompressible flow or conditions at exit of jet mixing region

j conditions in jet mixing region

m conditions in mixing region

p flat plate

R conditions in recompression region

r conditions at entrance of recompression region

s stagnation conditions

u conditions at upper jet boundary

w conditions at wall

∞ free stream approaching the step

Superscript:

n integer

A bar over a symbol denotes a nondimensional value; a tilde denotes a mean value. An asterisk denotes that the value has been normalized by the reference values. Primes denote differentiation with respect to ζ.

PHYSICAL MODEL

As a flow model to be analyzed, consider a two-dimensional rearward-facing slot followed with an infinite flat plate placed in a uniform supersonic stream. To simplify the analysis, the coolant flow is assumed to consist of the same species as the main stream and to be injected at mean subsonic velocity u_c and density ρ_c at the slot exit.

A schematic illustration of the characteristic flow pattern is shown in figure 1. Since the oncoming flow is supersonic, a Prandtl-Meyer fan emanates from the plate lip to deflect streamlines inward, and a separated boundary layer spreads itself downstream like a free jet. Inasmuch as the flow must become parallel to the flat plate far downstream, a recompression shock wave will make an appearance at some distance downstream of the slot, to deflect streamlines outward, and the viscous layer again attaches to the plate. When this simplified flow model is specified, the whole flow field can be divided into three regions. The first is a jet mixing region behind the point of

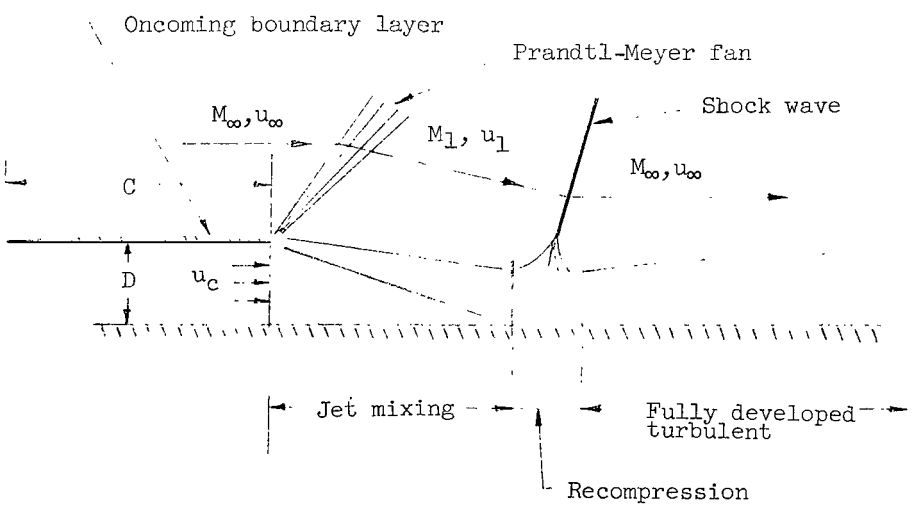

Figure 1.- Illustration of overall flow pattern.

separation, in which mixing between the external isentropic stream and internal dissipative flow determines the flow characteristics. The second is a recompression region next to the jet mixing region, in which an interaction between a shock wave and the viscous layer is the essential physical feature. Finally, there is an attached boundary layer along the flat plate downstream of the recompression region.

It is of primary interest to specify whether the separated viscous flow in the jet mixing region is laminar or turbulent. From the experimental point of view, it has already been reported in references 8 and 9 that the flow separation associated with an abrupt change of wall contour such as a rearward-facing step tends to induce transition a short distance downstream of the separation point even if the oncoming boundary layer is laminar. Of course, if the Reynolds number is sufficiently small, the separated viscous layer may be laminar. However, for practical applications, it seems realistic to assume that the separated viscous layer in the jet mixing region is turbulent except in the vicinity of the separation point, even with a laminar approaching boundary layer. Consequently, the viscous layer downstream is expected to remain turbulent throughout, although there is neither a rigorous theoretical proof nor an empirical criterion for this statement. If the oncoming boundary layer is turbulent, there is no doubt about this assumption.

TURBULENT JET MIXING REGION

The essential feature of the flow in this region is viscous mixing following flow separation at the edge of the plate lip. Therefore, mass, momentum, and energy transport through mixing between the external isentropic stream and internal dissipative flow play an important role in determining the flow field. This statement means that in contrast to the usual Prandtl boundary-layer theory, the external flow cannot be regarded as a known datum for calculating internal dissipative flow; rather, the development of dissipative flow itself helps to determine the external flow. In fact, the experimental results presented in reference 4 show that the strength of the Prandtl-Meyer fan decreases fairly rapidly with increase of the coolant flow rate. Consequently, the Mach number of the external flow changes with the coolant flow rate. This condition, in turn, changes the strength of the associated recompression shock wave which is again felt by the jet mixing layer through the dead-air region. Thus, the injection of coolant flow through a rearward-facing step-like slot involves a complicated flow mechanism of interaction in the jet mixing region.

Analogous to the usual base pressure problem, the pressure behind a coolant slot may be expressed as a function of oncoming flow Mach number, thickness of oncoming boundary layer at the separation point, height of coolant slot and coolant mass flow rate, and so forth, such as

$$p_1 = f\left(M_\infty, \delta_\infty, D, \frac{\rho_c u_c}{\rho_\infty u_\infty}, \ldots\right) \tag{1}$$

Although much effort has been devoted to this problem, there does not exist any general analytical approach suitable for estimating the pressure rigorously. The main reason is the difficulty of treating the viscous interaction mentioned in the previous paragraph, since, both in theory and in experiment, information on detailed flow structure in the dead-air region is meager. Besides, if the flow in the jet mixing region is specified as turbulent, another difficulty is that no fundamental equation is available. This problem, in turn, makes it necessary to introduce some empirical information or assumptions in any theoretical approach to the jet mixing region in general. Thus, it seems hopeless to develop an exact approach to the problem under consideration.

In spite of these difficulties, however, there is some empirical information pertinent to flow phenomena in the jet mixing region. Chapman et al. (ref. 9) pointed out from their experiments that an isentropic supersonic flow outside the dissipative region associated with flow separation behind a rearward-facing step can be considered to be approximately uniform. Exactly speaking, there must be some pressure gradient in the mixing region. However, intuitively, this pressure gradient is very small compared with that in the recompression region; therefore, an assumption of constant pressure at the edge of mixing layer is reasonable.

Moreover, if the thickness of the mixing layer is small, the usual boundary-layer approximations may be applicable to the jet mixing region. Based on this approximation, reference 10 presents a momentum equation for incompressible turbulent mixing by use of Prandtl's mixing length hypothesis and obtains a similar solution for the velocity distribution across the mixing layer. This solution, if the value of a scale factor is chosen properly, is shown to be in good agreement with experimental results presented in reference 11. Furthermore, the experimental results of reference 8 for compressible turbulent jet mixing indicate that the theoretical velocity profile presented in reference 12 agrees well with the experiment, but the value of the scale factor is seriously influenced by the Mach number of the external flow. In reference 8, it is further commented, in spite of the similar solution being derived on the basis of a concept of zero thickness of the oncoming boundary layer, that the similar velocity profile agrees well with experimental data, even in the case of nonzero thickness of the oncoming boundary layer.

It must be noted that although the experimental evidence may justify the applicability of the assumption of a similar flow field even in the case of nonzero thickness of the oncoming boundary layer, this assumption does not imply that the oncoming boundary layer has no influence on the flow characteristics in the jet mixing region. In fact, as will be shown later, the basic equations governing this region involve the Mach number of the external flow explicitly. Since the Mach number and, consequently, the associated

pressure in the jet mixing region are influenced by the thickness of the oncoming boundary layer and, in particular, this trend is strongest for the laminar approaching boundary layer, the flow characteristics in the jet mixing region depend clearly upon the oncoming boundary-layer thickness.

This empirical evidence suggests the possibility of developing an approximate analytical approach to compressible turbulent jet mixing by using a concept of similar solutions, even in the case of nonzero thickness of the oncoming boundary layer. However, it must be noted that from a mathematical viewpoint, this similar solution is an asymptotic form of an exact solution far downstream of the separation point and, therefore, it is not expected that it can predict the flow field accurately just downstream of the separation point.

The following section brings out the importance of the transport of mass, momentum, and energy from the outer stream to internal dissipative flow in determining the flow pattern in the jet mixing region and formulates this concept in quantitative terms on the basis of a simplified flow model. The basic assumptions are summarized as follows:

(1) Oncoming boundary layer is either laminar or turbulent and is thin compared with the step height, whereas the flow in the jet mixing region is turbulent except in the vicinity of the separation point where the oncoming boundary layer is laminar

(2) The pressure gradient in the jet mixing region is negligible

(3) The turbulent Prandtl number is constant

Analysis

Before proceeding with the analytical development, a coordinate system related to the mixing region and a condition inside the dead-air region must be specified. Unfortunately, there cannot be found, a priori, any definite intrinsic boundary within the mixing layer to which a physical coordinate system is referred. However, if the assumption of a similar flow field is introduced, it provides a characteristic streamline in the mixing layer along which physical properties are kept constant. Therefore, in the present approach, the x-axis of the coordinate system (x,y) is taken along this characteristic streamline with its origin at the point of separation, the y-axis being normal to the x-axis. However, it must be noted that the location of the characteristic streamline relative to the wall is not known a priori.

A condition inside the dead-air region is another point of interest. If coolant mass is injected into the dead-air region through a rearward-facing slot, the coolant flow must have, on the average, a finite nonzero velocity at the slot exit. As it flows downstream, mixing occurs between separated boundary-layer flow and the coolant flow by the "scavenging" effect. However, since the wall exists, growth of the mixing layer is

restricted and the coolant flow near the wall will be decelerated by viscous forces far downstream of the injection point. Thus, when the end of the jet-mixing region is approached, it can be expected that the mixing has almost finished and the separated boundary layer is ready for reattachment.

Therefore, near the end of the jet mixing region, the mixing layer has grown to the extent of almost the entire cross section of the dissipative flow, and the velocity profile must be nearly similar to that at the separation point.

On the other hand, since detailed flow structure in the dead-air region is ignored, it is intended in the present approach to estimate overall aerodynamic characteristics pertinent to the jet mixing region by considering a mass, momentum, and energy balance within a control volume bounded by the cross section at the entrance and exit of this region. For this purpose, it is more important to evaluate velocity and enthalpy profiles across the dissipative layer in a realistic form at the exit of the jet mixing region rather than at the intermediate points. For this reason, $u = 0$ is assumed as a boundary condition inside the dead-air region to obtain a velocity profile of the separation type.

By Prandtl's mixing length hypothesis, local shearing stress and heat-transfer rate may be expressed as

$$\tau = \epsilon(x)\, \rho \frac{\partial u}{\partial y}$$

$$q = - \frac{\epsilon(x)}{N_{Pr,t}} \rho \frac{\partial h}{\partial y}$$

where $\epsilon(x)$ is the eddy kinematic viscosity which is defined as

$$\epsilon(x) = c_1 u_1 x$$

and where c_1 indicates a constant of proportionality. Thus, the differential equations for mass, momentum, and energy conservation may be written within the accuracy of the boundary-layer approximation as

$$\frac{\partial \rho u}{\partial x} + \frac{\partial \rho v}{\partial y} = 0 \tag{2}$$

$$\rho u \frac{\partial u}{\partial x} + \rho v \frac{\partial u}{\partial y} = \epsilon(x) \frac{\partial}{\partial y}\left(\rho \frac{\partial u}{\partial y}\right) \tag{3}$$

$$\rho u \frac{\partial h}{\partial x} + \rho v \frac{\partial h}{\partial y} = \frac{\epsilon(x)}{N_{Pr,t}} \frac{\partial}{\partial y}\left(\rho \frac{\partial h}{\partial y}\right) + \epsilon(x)\left(\rho \frac{\partial u}{\partial y}\right)^2 \tag{4}$$

where all physical quantities indicate time-mean values.

The continuity equation may be accounted for by introducing a stream function

$$\frac{\partial \psi}{\partial x} = -\rho v$$

$$\frac{\partial \psi}{\partial y} = \rho u$$

Introducing the nondimensional expressions

$$x^* = \frac{x}{L}$$

$$u^* = \frac{u}{u_1}$$

$$h^* = \frac{h}{h_1}$$

$$\rho^* = \frac{\rho}{\rho_1}$$

$$\psi^* = \frac{\psi}{\sqrt{\rho_1 \mu_1 u_1 L}}$$

$$N_{Re,L} = \frac{u_1 L}{\nu_1}$$

and rewriting equations (3) and (4) then yields

$$\frac{\partial u^*}{\partial x^*} = \epsilon^* x^* \frac{\partial}{\partial \psi^*}\left(\frac{u^*}{h^{*2}} \frac{\partial u^*}{\partial \psi^*}\right) \tag{5}$$

$$\frac{\partial h^*}{\partial x^*} = \frac{\epsilon^*}{N_{Pr,t}} x^* \frac{\partial}{\partial \psi^*}\left(\frac{u^*}{h^{*2}} \frac{\partial h^*}{\partial \psi^*}\right) + \epsilon^* x^* \frac{u^*}{h^{*2}}\left(\frac{\partial u^*}{\partial \psi^*}\right)^2 \frac{u_1^2}{h_1} \tag{6}$$

where

$$\epsilon^* = c_1 N_{Re,L} \tag{7}$$

and where a relation $\rho^* = 1/h^*$ has been employed.

To obtain similar solutions to equations (5) and (6), a similarity parameter based on the streamline coordinate is introduced as an independent variable and is given by

$$\zeta = \sigma_1 \frac{\psi^*}{x^*} \tag{8}$$

where σ_1 denotes a scale factor. Thus, the momentum and energy equations may be reduced to

$$-\zeta = \frac{du^*}{d\zeta} = \frac{d}{d\zeta}\left(\frac{u^*}{h^{*2}}\frac{du^*}{d\zeta}\right) \tag{9}$$

$$-\zeta\frac{dh^*}{d\zeta} = \frac{1}{N_{Pr,t}}\frac{d}{d\zeta}\left(\frac{u^*}{h^{*2}}\frac{dh^*}{d\zeta}\right) + (\gamma - 1)M_1{}^2\frac{u^*}{h^{*2}}\left(\frac{du^*}{d\zeta}\right)^2 \tag{10}$$

$$\sigma_1{}^2 = \frac{1}{c_1 N_{Re,L}} \tag{11}$$

The boundary conditions are given by

$$\left.\begin{aligned} u^* &= h^* = 1 && (\zeta = \infty)\\ u^* &= 0 && (\zeta = -\infty)\\ h^* &= h_w^* && (\zeta = -\infty) \end{aligned}\right\} \tag{12}$$

If the wall enthalpy is denoted by H_w, then,

$$h_w^* = \frac{H_w}{h_1} = \frac{H_w}{H_\infty}\left(1 + \frac{\gamma - 1}{2}M_1{}^2\right) \tag{13}$$

In the case where the turbulent Prandtl number equals unity, the energy equation can be readily integrated analytically with the assumption that local static enthalpy is a function of u^* only. The result is $(N_{Pr,t} = 1.0)$

$$h^* = -\frac{\gamma - 1}{2}M_1{}^2u^{*2} + \left(1 + \frac{\gamma - 1}{2}M_1{}^2\right)\left[\frac{H_w}{H_\infty} + \left(1 - \frac{H_w}{H_\infty}\right)u^*\right] \tag{14}$$

It remains to discuss the value of the scale factor σ_1 which must be determined empirically. In the case of incompressible jet mixing, it is shown that if a similarity parameter ξ is defined by the use of an intrinsic coordinate system x,y such as

$$\xi = \sigma\frac{y}{x}$$

then good correlation between the theoretical velocity profile presented in reference 10 and the experimental data of reference 11 can be obtained for $\sigma = 13.5$ (ref. 12). In the case of compressible jet mixing, it is further shown (ref. 8) that the experimental velocity profile across the mixing layer at $M_1 = 1.6$ can be well correlated with the theoretical profile proposed in reference 13 for incompressible jet mixing, if the value of σ is chosen to be 18. On the other hand, a formula for σ for compressible jet mixing which accounts for Mach number effects can be derived by fitting an equation to the data of reference 11 at $M_1 = 0$ and reference 8 at $M_1 = 1.6$. This scale factor is given by the equation

$$\sigma = 13.5 + 6.16M_1\sqrt{\frac{\gamma - 1}{2}}$$

On the other hand, since the similarity parameter ζ used in the present approach is based on a streamline coordinate, the associated scale factor σ_1 becomes different from that for the intrinsic coordinate system. However, it can be shown from reference 8 that the constant of proportionality involved in the eddy kinematic viscosity is inversely proportional to σ^2; that is,

$$c_1 \propto \frac{1}{\sigma^2}$$

From this relation together with equation (11) it is found that

$$\sigma_1\sqrt{N_{Re,L}} = \frac{1}{\sqrt{c_1}} \propto \sigma$$

Therefore, the scale factor σ_1 is given by the equation

$$\sigma_1\sqrt{N_{Re,L}} = X\left(13.5 + 6.16M_1\sqrt{\frac{\gamma - 1}{2}}\right) \tag{15}$$

where X denotes a constant of proportionality. Unfortunately, the value of X is not known rigorously. As will be shown in the subsequent section, the value of X depends strongly upon the value of a mixing coefficient which seems to play the most important role in determining the aerodynamic characteristics in the jet mixing region. Since there exists neither theoretical nor empirical information on rigorous evaluation of the mixing coefficient, it is assumed for the present that X is unity. To demonstrate the effect of X on flow characteristics, an example of the heat-transfer rate is calculated later for $X = 2$ and the results are compared with those for $X = 1$.

Equations (9) and (10) can be integrated by using an iteration scheme. Let

$$\frac{u^*}{h^{*2}} = f(\zeta) \tag{16a}$$

$$\frac{u^*}{h^{*2}}\frac{du^*}{d\zeta} = F(\zeta) \tag{16b}$$

$$\frac{u^*}{h^{*2}}\frac{dh^*}{d\zeta} = G(\zeta) \tag{16c}$$

Then solutions for u^* and h^* satisfying the given boundary conditions may be obtained, respectively, as (see appendix)

$$u^*(\zeta) = \hat{\beta}\int_{-\infty}^{\zeta}\frac{F}{f}\,d\zeta \tag{16d}$$

$$h^*(\zeta) = \frac{1 - h_w^* + \hat{\beta}^2 N_{Pr,t}(\gamma - 1)M_1^2 \int_{-\infty}^{\infty} \frac{F^{N_{Pr,t}}}{f} \int_0^{\xi} \frac{F^{2-N_{Pr,t}}}{f} d\eta\, d\xi}{\int_{-\infty}^{\infty} \frac{F^{N_{Pr,t}}}{f} d\zeta} \times \int_{-\infty}^{\zeta} \frac{F^{N_{Pr,t}}}{f} d\zeta$$

$$- \hat{\beta}^2 N_{Pr,t}(\gamma - 1)M_1^2 \int_{-\infty}^{\zeta} \frac{F^{N_{Pr,t}}}{f} \int_0^{\xi} \frac{F^{2-N_{Pr,t}}}{f} d\eta\, d\xi + h_w^* \qquad (17)$$

where

$$F(\zeta) = \exp\left(-\int_0^{\zeta} \frac{\zeta}{f} d\zeta\right)$$

$$\hat{\beta} = \frac{1}{\int_{-\infty}^{\infty} \frac{F}{f} d\zeta}$$

Numerical calculation is carried out by evaluating $f(\zeta)$, first, from assumed profiles for velocity and static enthalpy as a first-order approximation. Then, by use of the $f(\zeta)$ value thus obtained, the first-order velocity and enthalpy profiles are calculated from equations (16) and (17), respectively. With these values, the second-order approximation of $f(\zeta)$ is obtained and the same calculation procedure is repeated until solutions for u^* and h^* converge sufficiently.

Mass and Momentum Balance at Exit of Jet Mixing Region

Although the rate of spread of the mixing layer itself is known from the value of the scale factor, the location of the characteristic streamline ($\zeta = 0$) relative to the wall is not known a priori. However, it may be determined by considering the transport of mass and momentum from the external stream to the internal dissipative flow.

It is clear that in the jet mixing region, there are two physically important boundaries other than the characteristic streamline. One is the upper jet boundary which separates the region of internal dissipative flow from the external isentropic supersonic stream. Another is the so-called "dividing streamline" which separates the mass of fluid originally in the oncoming flow from the coolant flow. However, at a free boundary such as jet boundary, any physical quantity in the dissipative region must approach asymptotically the value of the outer flow; thus, there is no intrinsically distinct boundary between the dissipative region and the external flow. Because of this, the upper jet boundary is defined in the present approach as the loci of points where $u^* = 0.99$.

Simple sketches of the characteristic flow pattern shown in figure 2 may be helpful for subsequent development. From conservation of mass it is easily shown that the mass of fluid entering across segment $\overline{AB}$ (fig. 2) must be equal to that leaving across segment $\overline{CF}$ at the exit of mixing region ($x = L$ or $x^* = 1$); that is,

$$\left(\int_{y_d}^{y_u} \rho u \, dy\right)_{x=L} = \rho_1 u_1 (y_u - y_m - \delta_1) + \rho_1 u_1 (\delta_1 - \delta_1^*)$$

The first term on the right-hand side of the preceding equation indicates the mass of fluid entrained in the control volume $\overline{ABCF}$ from outer inviscid flow through mixing, and

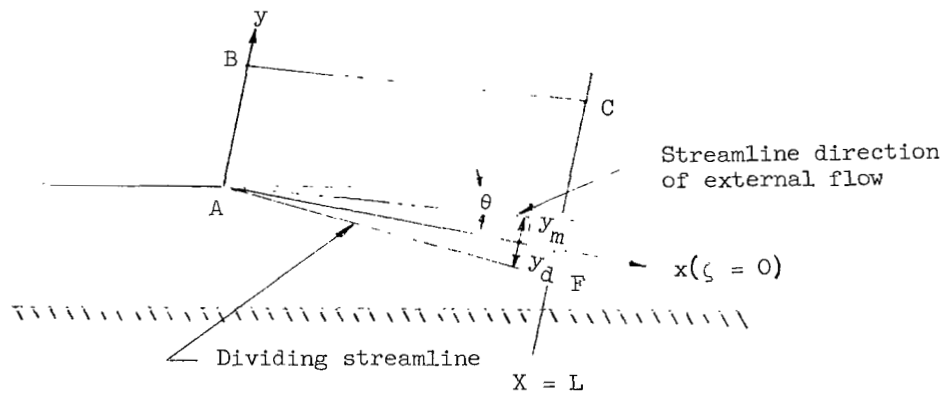

(a)

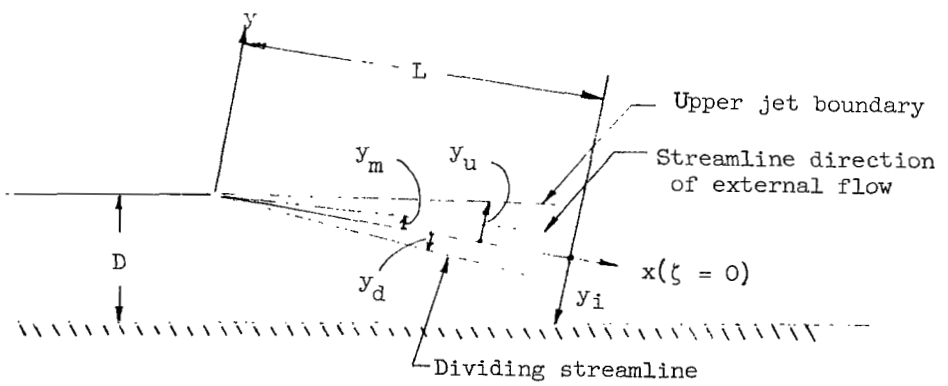

(b)

Figure 2.- Characteristic flow field near exit of jet mixing region.

the second term denotes the mass of fluid originally existing in the oncoming boundary layer. Thus, the preceding equation may be reduced by use of nondimensional expressions to

$$\int_{\zeta_m}^{\zeta_u} \frac{h^*}{u^*}\, d\zeta = \zeta_u - \zeta_d + \sigma_1\sqrt{N_{Re,L}}\,\frac{\delta_1^*}{L} \tag{18}$$

From the definition of the dividing streamline, the mass of coolant flow entrained in the mixing region must exist in a region between the dividing streamline and the wall (fig. 2); that is,

$$\rho_c u_c D = \left(\int_{y_i}^{y_d} \rho u\, dy\right)_{x=L}$$

which can be reduced to

$$\rho_c{}^* u_c{}^* \frac{D}{L} = \frac{\zeta_d - \zeta_i}{\sigma_1\sqrt{N_{Re,L}}} \tag{19}$$

On the other hand, the momentum of fluid involved in the viscous layer at $x = L$ may be expressed as the sum of the momentum entrained in the viscous region from external flow by mixing, and the work done on the gas due to shearing stress at the wall; that is,

$$\int_{y_i}^{y_u} \rho u^2 dy = \rho_1 u_1{}^2\left(\delta_1 - \delta_1{}^* - \theta_1{}^*\right) + u_1\left[\int_{y_d}^{y_u} \rho u\, dy - \rho_1 u_1\left(\delta_1 - \delta_1{}^*\right)\right]$$

$$+ u_c \int_{y_i}^{y_d} \rho u\, dy - \tilde{\tau}_{w,j} L$$

where $\tilde{\tau}_{w,j}$ denotes mean shearing stress on the wall. The first term on the right-hand side of the preceding equation indicates the contribution from the oncoming boundary layer and the second and third terms denote momentum entrained from external isentropic flow and coolant flow, respectively. The last term is the work done by gas on the wall. By use of nondimensional expressions, the equation may be reduced to

$$\int_{\zeta_i}^{\zeta_u} u^* d\zeta = \zeta_u - u_c{}^*\zeta_i - \left(1 - u_c{}^*\right)\zeta_d - \sigma_1\sqrt{N_{Re,L}}\left(\frac{\theta_1{}^*}{L} + \frac{1}{2}\,\tilde{C}_{f,j}\right) \tag{20}$$

where

$$\tilde{C}_{f,j} = \frac{\tilde{\tau}_{w,j}}{\frac{1}{2}\rho_1 u_1{}^2}$$

Moreover, from the geometry, one can obtain an approximate expression such as (see fig. 2)

$$D \approx L \sin(\theta + \epsilon) + |y_i| \approx L(\theta + \epsilon) + |y_i|$$

where

$$\tan \epsilon \approx \epsilon \approx \frac{y_m}{x} = \frac{1}{\sigma_1 \sqrt{N_{Re,L}}} \int_0^{\zeta_m} \frac{h^*}{u^*} \, d\zeta$$

$$|y_i| = \frac{L}{\sigma_1 \sqrt{N_{Re,L}}} \int_{\zeta_i}^{0} \frac{h^*}{u^*} \, d\zeta$$

and hence

$$\frac{D}{L} = \theta + \frac{1}{\sigma_1 \sqrt{N_{Re,L}}} \left[J(\zeta_m) - J(\zeta_i) \right] \tag{21}$$

where

$$J(\zeta) = \int_0^{\zeta} \frac{h^*}{u^*} \, d\zeta \tag{22}$$

Thus, elimination of ζ_d and L from equations (18), (20), and (21) gives

$$-\left[(1 - u_c^*) \left(1 + \frac{\delta_1^*}{D} \right) + \frac{\theta_1^*}{D} \right] J(\zeta_m)$$

$$= \int_{\zeta_i}^{\zeta_u} u^* \, d\zeta - (1 - u_c^*) J(\zeta_u) - u_c^* (\zeta_u - \zeta_i)$$

$$+ \left[(1 - u_c^*) \frac{\delta_1^*}{D} + \frac{\theta_1^*}{D} \right] \left[\sigma_1 \sqrt{N_{Re,L}} \theta - J(\zeta_i) \right] + \frac{1}{2} \sigma_1 \sqrt{N_{Re,L}} \tilde{C}_{f,j} \tag{23}$$

In the case of no coolant flow, where $u_c^* = 0$ and $\zeta_d = \zeta_i$, equation (20) is further reduced with the aid of the mass balance equation (eq. (18)) to

$$\int_{\zeta_d}^{\zeta_u} u^* \, d\zeta = \zeta_u - \zeta_d - \frac{\theta_1^*}{D} \left[\sigma_1 \sqrt{N_{Re,L}} \theta + J(\zeta_m) - J(\zeta_d) \right] - \frac{1}{2} \sigma_1 \sqrt{N_{Re,L}} \tilde{C}_{f,j} \tag{24}$$

and the mass balance equation may be reexpressed by use of equation (22) as

$$\zeta_d = \zeta_u - J(\zeta_u) + \left(1 + \frac{\delta_1^*}{D} \right) J(\zeta_m) + \frac{\delta_1^*}{D} \left[\sigma_1 \sqrt{N_{Re,L}} \theta - J(\zeta_i) \right] \tag{25}$$

In the preceding equations, δ_1^* and θ_1^* indicate displacement thickness and momentum thickness of the entrained boundary layer just downstream of Prandtl-Meyer fan and can be connected with those of the oncoming boundary layer when mass and momentum conservation of boundary-layer flow through the Prandtl-Meyer expansion is assumed; that is,

$$\rho_1 u_1 \left(\delta_1 - \delta_1^*\right) = \rho_\infty u_\infty \left(\delta_\infty - \delta_\infty^*\right)$$

$$\rho_1 u_1^2 \left(\delta_1 - \delta_1^* - \theta_1^*\right) = \rho_\infty u_\infty^2 \left(\delta_\infty - \delta_\infty^* - \theta_\infty^*\right)$$

Since the state of the boundary layer will not change through a Prandtl-Meyer fan irrespective of whether the oncoming boundary layer is laminar or turbulent, δ_1^*/δ_1 and θ_1^*/δ_1 will not change much from $\delta_\infty^*/\delta_\infty$ and $\theta_\infty^*/\delta_\infty$, respectively. Thus, rather simple conservation equations such as

$$\rho_1 u_1 \delta_1^* = \rho_\infty u_\infty \delta_\infty^*$$

$$\rho_1 u_1^2 \theta_1^* = \rho_\infty u_\infty^2 \theta_\infty^*$$

can be applied. Therefore,

$$\left.\begin{aligned} \frac{\delta_1^*}{D} &= \frac{\rho_\infty u_\infty}{\rho_1 u_1} \frac{\delta_\infty^*}{D} = \frac{M_\infty}{M_1} \left[\frac{2 + (\gamma - 1) M_1^2}{2 + (\gamma - 1) M_\infty^2}\right]^{\frac{\gamma+1}{2(\gamma-1)}} \frac{\delta_\infty^*}{D} \\ \frac{\theta_1^*}{D} &= \frac{\rho_\infty u_\infty^2}{\rho_1 u_1^2} \frac{\delta_\infty^*}{D} = \frac{M_\infty^2}{M_1^2} \left[\frac{2 + (\gamma - 1) M_1^2}{2 + (\gamma - 1) M_\infty^2}\right]^{\frac{\gamma}{\gamma-1}} \frac{\theta_\infty^*}{D} \end{aligned}\right\} \tag{26}$$

Now δ_∞^* and θ_∞^* can be expressed in terms of Reynolds number referred to the oncoming flow conditions for either laminar or turbulent approaching boundary layers by equations such as

$$\left.\begin{aligned} \frac{\delta_\infty^*}{D} &= K_D \frac{C}{D \sqrt[n]{N_{Re}}} = K_D Z \\ \frac{\theta_\infty^*}{D} &= K_M \frac{C}{D \sqrt[n]{N_{Re}}} = K_M Z \end{aligned}\right\}$$

(Equations continued on next page)

$$\left.\begin{aligned} Z &= \frac{C}{D\sqrt[n]{N_{Re}}} \\ N_{Re} &= \frac{u_\infty C}{\nu_\infty} \end{aligned}\right\} \qquad (27)$$

Equations (24) and (25) can be considered as simultaneous equations with respect to Z and $J(\zeta_m)$, where $n = 2$ for the laminar oncoming boundary layer and $n = 5$ for the turbulent oncoming boundary layer. In the preceding equation K_D and K_M are constants of proportionality associated with displacement thickness and momentum thickness, respectively. Their values are, of course, changed depending upon whether the oncoming boundary layer is laminar or turbulent.

Thus, in the case of no coolant flow $(u_c^* = 0)$, Z is known for given conditions if $\zeta_d(= \zeta_i)$ is known. Since the oncoming boundary layer is not influenced by coolant mass injection, the value of Z must be kept constant for the coolant flow case. Therefore, δ_1^*/D and θ_1^*/D are known for each coolant flow case and with these values $J(\zeta_m)$ and ζ_d are determined by using equations (23) and (25) if ζ_i is known. The procedure for this calculation is described in detail in a later section. In any case, it seems necessary, first of all, to know the value of ζ_i. Unfortunately, solutions appropriate to the jet mixing region do not give any information on ζ_i; therefore, it must be determined from recompression conditions. As is well-known, since a complicated interaction between a shock wave and a turbulent boundary layer is the essential physical feature in the recompression region, it seems hopeless to develop any rigorous approach to this interaction phenomenon. To avoid this difficulty, reference 14 proposes an intuitive criterion for penetration of fluid particles through the recompression region. This criterion may be expressed in the statement that at the entrance of recompression region, the fluid must, at least, have a level of mechanical energy equal to the static pressure behind the shock; as a result, the recompression to that static pressure is possible by complete conversion of the kinetic energy isentropically. Although there is no rigorous proof for this statement, this criterion could be used. However, this method underestimates the value of ζ_i, since the effect of viscous dissipation in the recompression region is neglected. Because of this underestimation, ζ_i in the present approach will be evaluated from a condition of mass flow conservation between the jet mixing region and the recompression region, and will be discussed briefly in a later section. For this purpose, it may be helpful to present a mass-flow relation at the exit of the jet mixing region,

$$\left(\int_{y_i}^{y_u} \rho u \, dy\right)_{x=L} = \rho_1 u_1 L \frac{\zeta_u - \zeta_i}{\sigma_1\sqrt{N_{Re,L}}} \qquad (28)$$

The fact that equations (23) and (25) involve δ_1^*/D and θ_1^*/D clearly indicates that physical properties in the jet mixing region, such as pressure and the length of the separated region, depend upon the ratio of oncoming boundary-layer thickness to coolant slot height. This dependence, in turn, means that such properties can be correlated to the parameter Z as in the case of the usual base pressure problem, and thus the correlation found in reference 15 is confirmed.

The value of mean skin-friction coefficient $\tilde{C}_{f,j}$ will now be considered. Since detailed flow structure near the wall is ignored, $\tilde{C}_{f,j}$ cannot be estimated in the conventional way; therefore, in the present approach, it is evaluated by use of an approximate semiempirical method. For this purpose it is convenient to introduce a concept of a mixing coefficient originally proposed in reference 16 which is defined as

$$\frac{d\tilde{m}_j}{dx} = K_j \rho_1 u_1$$

where K_j is the mixing coefficient and $\tilde{m}_j$ denotes mass of fluid entrained in the mixing layer from external isentropic flow. The left-hand side of the preceding equation may be expressed by

$$\frac{d\tilde{m}_j}{dx} = \frac{d}{dx}\int_0^{y_u} \rho u \, dy = \frac{\rho_1 u_1 \zeta_u}{\sigma_1 \sqrt{N_{Re,L}}}$$

Therefore,

$$K_j = \frac{\zeta_u}{\sigma_1 \sqrt{N_{Re,L}}} \tag{29}$$

If the parameter ϕ is defined for a general state of the viscous layer as

$$\phi = \frac{C_f}{2K(1 - \kappa)}$$

where C_f and K denote local skin-friction coefficient and mixing coefficient, respectively, and κ is a parameter defined by

$$\kappa = \frac{\delta - \delta^* - \theta^*}{\delta - \delta^*}$$

then, $\tilde{C}_{f,j}$ may be given in a form

$$\tilde{C}_{f,j} = 2K_j\left(1 - \tilde{\kappa}_j\right)\tilde{\phi}_j = \frac{2\zeta_u\left(1 - \tilde{\kappa}_j\right)}{\sigma_1 \sqrt{N_{Re,L}}}\tilde{\phi}_j \tag{30}$$

where $\tilde{\kappa}_j$ and $\tilde{\phi}_j$ denote their mean values in the jet mixing region. In the case of an incompressible turbulent boundary layer on a flat plate, it is easily shown that $\phi = 1$. In general, for any other boundary-layer state, there exists no useful method to estimate ϕ. The same difficulty is found in the evaluation of $\tilde{\kappa}_j$. For this reason, $\tilde{\kappa}_j$ is assumed to be replaceable by the value obtained at the entrance of the recompression region; that is,

$$\tilde{\kappa}_j \approx \tilde{\kappa}_r$$

On the other hand, the value of $\tilde{\phi}_j$ seems to depend mainly upon local dynamic pressure and wall enthalpy. However, since it seems almost impossible to obtain a functional dependency of $\tilde{\phi}_j$ on dynamic pressure and wall enthalpy analytically, the base pressure behind a two-dimensional rearward-facing step $\left(u_c^* = 0\right)$ was calculated for $M_1 = 1.5$ and 2.0 under the assumption that the base pressure is rather insensitive to wall enthalpy. Several sets of parameters $\left(M_\infty, M_1, \tilde{\phi}_j\right)$, which can be correlated to the experimental data shown in reference 15, were found by use of a trial-and-error method. The values of these parameters thus obtained correlate through an equation

$$\tilde{\phi}_j = 9.68 \frac{S(M_\infty)}{S(M_1)} \exp\left(-M_\infty^{3/2}\right)\left[1 + 15.93\left(1 - \frac{H_w}{H_\infty}\right)\right] \tag{31}$$

where

$$S(M) = \frac{1}{2}\gamma M^2\left(1 + \frac{\gamma - 1}{2} M^2\right)^{-\frac{\gamma}{\gamma-1}}$$

Thus, the final term on the right-hand side of equation (23) or equation (24) is given as

$$\frac{1}{2}\sigma_1\sqrt{N_{Re,L}}\,\tilde{C}_{f,j} = \zeta_u\left(1 - \tilde{\kappa}_j\right)\tilde{\phi}_j \tag{32}$$

It must be noted that equation (31) is an approximate empirical formula for $\tilde{\phi}_j$; any future rigorous evaluation of the mean-skin friction coefficient in the jet mixing region will improve the present approach.

From the foregoing analysis, physical properties in the jet mixing region such as, for example, the pressure, can be expressed as a function of oncoming flow Mach number, ratio of oncoming boundary-layer thickness to slot height, and coolant flow rate; that is

$$p_1 = f\left(M_\infty, \frac{C}{D\sqrt[n]{N_{Re,L}}}, \frac{\rho_c u_c}{\rho_\infty u_\infty}, \frac{H_w}{H_\infty}\right)$$

and this equation is an alternate form of equation (1).

However, it should be noted that the present approach involves the value of ζ_u explicitly and obviously depends upon the definition of the upper jet boundary. This condition clearly indicates that the solution to the jet mixing region depends, to a certain extent, upon the definition of ζ_u. Unfortunately, there is no rigorous way to avoid this uncertainty. The present approach could be improved with a rigorous definition of ζ_u as well as $\tilde{C}_{f,j}$.

It is convenient for subsequent development to introduce a coolant flow rate, normalized by the oncoming flow conditions, which is defined as

$$\dot{M} = \frac{\rho_c u_c}{\rho_\infty u_\infty}$$

This equation can be reexpressed by use of local flow conditions in the jet mixing region in a form

$$\dot{M} = \rho_c{}^* u_c{}^* \frac{M_\infty}{M_1}\left[\frac{2 + (\gamma - 1)M_1{}^2}{2 + (\gamma - 1)M_\infty{}^2}\right]^{\frac{\gamma+1}{2(\gamma-1)}} \tag{33}$$

Energy Balance and Heat-Transfer Rate

Estimation of heat-transfer rate in the jet mixing region is another important problem. As has already been mentioned, the detailed flow structure near the wall is ignored in this region; therefore, conventional methods cannot be applied to calculate the local heat-transfer rate to the wall. However, it is possible to evaluate a mean heat-transfer rate by considering an energy balance within a control volume in the mixing region.

Consider a control volume enclosed by a surface S which consists of the characteristic streamline $\overline{AB}$, the entrance $\overline{DA}$, and the exit $\overline{BC}$ of the mixing region, and the wall $\overline{CD}$. (See fig. 3.) Since flow is assumed to be steady, the sum of heat input Q

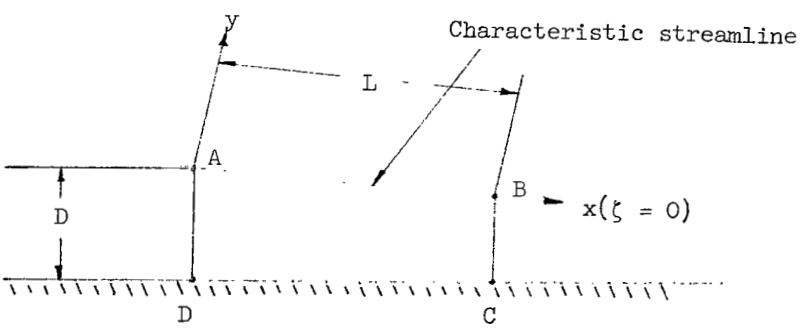

Figure 3.- Control surface for energy balance.

across S, the increase in internal energy and kinetic energy within S, the work W_p done on the gas through pressure normal to S, and the work W_S done on the gas through shearing stress on S must be zero; that is,

$$Q + E + W_p + W_S = 0 \tag{34}$$

Each term is given as follows:

$$\left.\begin{aligned} Q &= \iint_S q \, dS \\ E &= \iint_S \left(e + \frac{V^2}{2}\right)\rho V_n \, dS = \iint_S \left(h + \frac{V^2}{2}\right)\rho V_n \, dS + \iint_S pV_n \, dS \\ W_p &= \iint_S p(-V_n) \, dS \\ W_S &= \iint_S \tau V_t \, dS \end{aligned}\right\} \tag{35}$$

where the subscripts n and t denote the outward directed normal component and the tangential component to S, respectively. Before the estimation of each integral term, it is helpful to clarify conditions and assumptions imposed on S, which may be summarized as follows:

(1) $V_n = 0$ along $\overline{AB}$ and $\overline{CD}$

(2) $V_t = 0$ along $\overline{CD}$

(3) V_t is negligible along $\overline{BC}$ and $\overline{DA}$ and

(4) $\frac{\partial T}{\partial n}$ is negligible along $\overline{BC}$ and $\overline{DA}$

With these conditions the first integral can be expressed as

$$Q = \int_0^L \left[\frac{\epsilon(x)}{N_{Pr,t}} \rho \frac{\partial h}{\partial y}\right]_{y=0} dx - \tilde{q}_{w,j} L$$

where $\tilde{q}_{w,j}$ denotes mean heat-transfer rate to the wall. This equation is further reduced to

$$Q = \frac{\rho_1 u_1 h_1 L}{N_{Pr,t} \sigma_1 \sqrt{N_{Re,L}}} \left(\frac{u^*}{h^{*2}} \frac{dh^*}{d\zeta}\right)_{\zeta=0} - \tilde{q}_{w,j} L$$

where the first term on the right-hand side of the equation indicates heat input into the control volume across $\overline{AB}$ due to conduction. The sum of the second and the third integrals in equations (35) may be expressed as

$$E + W_p = \rho_c u_c H_c D + \int_{y_d}^{0} (\rho u H)_{x=0}\, dy - \int_{y_i}^{0} (\rho u H)_{x=L}\, dy$$

The first and the second terms on the right-hand side of the preceding equation indicate energy inputs into the control volume due to coolant flow and oncoming boundary-layer flow, respectively, and the last term denotes the energy going out of the control volume across $\overline{BC}$. The last integral in equations (35), which indicates heat generation due to viscous effects, may be written in a form

$$W_S = \int_0^L \left[\epsilon(x)\, \rho u \frac{\partial u}{\partial y}\right]_{y=0} dx = \frac{\rho_1 u_1 h_1 L}{\sigma_1 \sqrt{N_{Re,L}}} (\gamma - 1) M_1^2 \left(\frac{u^{*2}}{h^{*2}} \frac{du^*}{d\zeta}\right)_{\zeta=0}$$

Therefore, equation (34) can be expressed as

$$\int_0^L \left[\frac{\epsilon(x)}{N_{Pr,t}} \rho \frac{\partial h}{\partial y}\right]_{y=0} dx - \tilde{q}_{w,j} L + \rho_c u_c H_c D + \int_{y_d}^{0} (\rho u H)_{x=0}\, dy$$

$$- \int_{y_i}^{0} (\rho u H)_{x=L}\, dy + \int_0^L \left[\epsilon(x)\, \rho u \frac{\partial u}{\partial y}\right]_{y=0} dx = 0 \tag{36}$$

On the other hand, mass continuity within the control volume gives a relation

$$\rho_c u_c D + \int_{y_d}^{0} (\rho u)_{x=0}\, dy - \int_{y_i}^{0} (\rho u)_{x=L}\, dy = 0 \tag{37}$$

where the first and the second terms on the left-hand side of equation (37) indicate mass fluxes entrained in the control volume from coolant flow and oncoming boundary-layer flow, respectively, and the last term denotes mass flux going out of the control volume and across $\overline{BC}$. Multiplying equation (37) by H_∞ and subtracting the result from equation (36), $(H)_{x=0} = H_\infty$ being assumed and the nondimensional expressions being introduced, then yields the mean heat-transfer rate in the jet mixing region as

$$\frac{\tilde{q}_{w,j}}{\rho_1 u_1 h_1} = \frac{1}{\sigma_1 \sqrt{N_{Re,L}}} \left[\frac{1}{N_{Pr,t}} \left(\frac{u^*}{h^{*2}} \frac{dh^*}{d\zeta}\right)_{\zeta=0} + (\gamma - 1) M_1^2 \left(\frac{u^{*2}}{h^{*2}} \frac{du^*}{d\zeta}\right)_{\zeta=0}\right.$$

$$\left. - \frac{H_\infty}{h_1}\left(1 - \frac{H_c}{H_\infty}\right)(\zeta_d - \zeta_i) - \frac{H_\infty}{h_1} \zeta_i - \int_{\zeta_i}^{0} \left(h^* + \frac{\gamma - 1}{2} M_1^2 u^{*2}\right) d\zeta\right] \tag{38}$$

In the case of $N_{Pr,t} = 1.0$, this equation can be further simplified with the aid of equation (14) to

$$\frac{\tilde{q}_{w,j}}{\rho_1 u_1 H_\infty} = \frac{1}{\sigma_1 \sqrt{N_{Re,L}}}\left(1 - \frac{H_w}{H_\infty}\right)\left[\left(\frac{u^*}{h^{*2}}\frac{du^*}{d\zeta}\right)_{\zeta=0} - \zeta_i - \int_{\zeta_i}^{0} u^* \, d\zeta \right.$$

$$\left. - \frac{H_\infty - H_c}{H_\infty - H_w}\left(\zeta_d - \zeta_i\right)\right] \tag{39}$$

where the final term in the bracket of equation (39) indicates that the coolant mass reduces the heat-transfer rate as a heat sink.

If the mean heat-transfer coefficient $\tilde{C}_{q,j}$ in the jet mixing region is defined as

$$\tilde{C}_{q,j} = \frac{\tilde{q}_{w,j}}{\rho_\infty u_\infty H_\infty} \tag{40}$$

then

$$\tilde{C}_{q,j} = \frac{\rho_1 u_1}{\rho_\infty u_\infty}\frac{\tilde{q}_{w,j}}{\rho_1 u_1 H_\infty} = \frac{M_1}{M_\infty}\left[\frac{2 + (\gamma - 1)M_\infty^2}{2 + (\gamma - 1)M_1^2}\right]^{\frac{\gamma+1}{2(\gamma-1)}}\frac{\tilde{q}_{w,j}}{\rho_1 u_1 H_\infty} \tag{41}$$

In contrast to conventional boundary-layer transpiration cooling, in which the Mach number of the external flow is rather insensitive to coolant flow rate, with coolant injection the external flow Mach number in the jet mixing region is fairly sensitive to the coolant mass injection. Furthermore, this characteristic is an unfavorable factor in the reduction of heating rate in the jet mixing region, since M_1 decreases with an increase in the coolant flow rate. This decrease, in turn, tends to increase $\tilde{C}_{q,j}$, as is seen in equation (41), and this fact may be largely responsible for the marked difference in heat-transfer rate between separated flow and attached boundary-layer flow.

Despite the unfavorable factor just mentioned, the film cooling of the present type is still effective in reducing heat transfer in the region farther downstream of the separation point because a large amount of mass transport, induced by the strong action of jet mixing, can certainly be expected from the external flow to the internal dissipative flow. This process increases the thickness of the boundary layer downstream and reduces the heating rate to some extent.

RECOMPRESSION REGION

One of the most interesting phenomena in fluid mechanics, which is, in an exact sense, still unsolved, is the interaction between a shock wave and a viscous layer. This

interaction can be observed in many practical problems of supersonic flow, such as base pressure behind blunt-based bodies and the flow separation associated with recompression in an overexpanded supersonic nozzle.

Although many attempts have been made to clarify the aerodynamic mechanism of this phenomenon by both theoretical and experimental methods, there does not seem to exist any analytical approach pertinent to internal and external flow characteristics from which appreciable information is available. The main reason for this deficiency is the fact that application of the conventional boundary-layer approximations has been recognized to be doubtful for this kind of interaction phenomenon.

Since it seems hopeless to attempt to solve the complete Navier-Stokes equations in detail, reference 16 presents an approximate analytical theory of shock-wave—boundary-layer interaction without heat transfer derived by modifying the von Kármán momentum integral method with emphasis being laid on the importance of mass transport from the outer nearly isentropic stream to the internal dissipative flow through mixing.

In this interaction, it is well-known that the external flow cannot be given a priori as a known datum for calculation of the internal dissipative flow. The development of dissipative flow itself must be fed back to determine the external flow. This interplay, which is now generally recognized as the basis of any valid theoretical treatment, seems to have been formulated successfully in reference 16 with the assumption that any state of the boundary layer might be predicted by a single parameter.

For the case of a compressible laminar boundary layer involving separation, the validity of this assumption is reasonably verified from the correlation of incompressible data through the Illingworth-Stewartson transformation. (See ref. 12.) However, if the boundary layer is specified as turbulent, nothing of this kind can be done rigorously because of the almost complete lack of theoretical knowledge on the effect of compressibility, and also because even the empirical information in the incompressible case is meager. Despite much discussion on the possibility of considering physical properties associated with an incompressible turbulent boundary layer as a one-parameter family, it is not yet clear whether this assumption in general is even approximately correct. However, if the physical properties do not change too fast, the assumption may be adequate.

Moreover, if heat transfer is involved in the problem, the real physical feature of the compressible turbulent boundary layer with a pressure gradient will become much more complicated because the energy equation should couple with the momentum equation. Since there is neither theoretical nor empirical information available for predicting the enthalpy profile across turbulent boundary layers, except for the flat-plate

case presented in reference 17, it seems impossible to solve the present problem without making some assumption concerning the enthalpy profile.

Introduction of the assumption of a one-parameter family of turbulent boundary layers provides a mean temperature within the layer from mass and momentum relations, as pointed out in reference 16. However, there is not any rigorous method available to examine whether this mean temperature is even approximately consistent with the energy equation.

The purpose of this section is to present an approximate approach to the shock-wave—turbulent-boundary-layer interaction with heat transfer so as to emphasize the importance of the transport of mass, momentum, and energy in determining the flow pattern. The present approach is essentially based on the one presented in reference 16 for shock-wave—boundary-layer interaction without heat transfer. The basic assumptions made in the present approach may be summarized as follows:

(1) Any state of the turbulent boundary layer with a pressure gradient may be predicted as a single-parameter family

(2) The static pressure across the internal viscous layer is constant and equal to the local pressure in the adjacent external flow

(3) The wall temperature is constant

(4) The turbulent Prandtl number is constant and equal to unity

(5) The total enthalpy profile across the boundary layer is assumed to be a function of local velocity u only and is given in the form

$$H = c_p T + \frac{1}{2} u^2 = \left(H_e - H_w\right)\frac{u}{u_e} + H_w \tag{42}$$

The final assumption has already been proved to be correct by Van Driest (ref. 17) for compressible turbulent boundary layer without pressure gradient if the turbulent Prandtl number is unity. In the general case, there is no rigorous proof for equation (42). However, it is expected to be approximately valid if the temperature profile within the boundary layer does not change too fast.

Analysis

To simplify the analysis, a shock wave is assumed to be replaceable by a family of isentropic compression waves. This assumption seems to be reasonable because the shock wave tends to be diffused and becomes a family of compression waves near the boundary layer. A simple sketch of the characteristic flow pattern in the recompression region is shown in figure 4. The flow field is assumed to consist of two regions, an

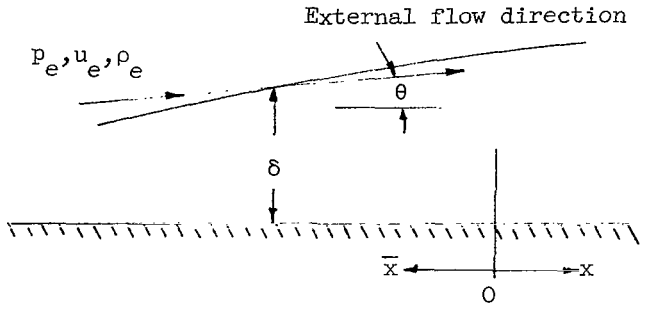

Figure 4.- Flow field in recompression region.

internal viscous layer of local thickness δ and an external nearly isentropic flow in which the local streamline makes the angle θ with the x-axis at $y = \delta$.

The basic equations governing the viscous layer are:

$$\frac{\partial \rho u}{\partial x} + \frac{\partial \rho v}{\partial y} = 0 \tag{43}$$

$$\rho u \frac{\partial u}{\partial x} + \rho v \frac{\partial u}{\partial y} = -\frac{\partial p}{\partial x} + \frac{\partial \tau}{\partial y} \tag{44}$$

$$\rho u \frac{\partial h}{\partial x} + \rho v \frac{\partial h}{\partial y} = -\frac{\partial q}{\partial y} + u \frac{\partial p}{\partial x} + \partial \frac{\partial u}{\partial y} \tag{45}$$

Although equation (45) is an energy equation, the solution of this equation has already been assumed to be given by equation (42). Therefore, it is not necessary to couple equation (45) with equation (44) in the present approach. Thus, equation (45) should be considered as an expression for obtaining the heat-transfer rate to the wall.

Before proceeding to a detailed analytical development, it may be helpful to define several physical quantities which will be used in the subsequent argument. Fluxes of mass, momentum, and energy across the viscous layer are expressed, respectively, as

$$\tilde{m} = \int_0^\delta \rho u \, dy = \rho_e u_e (\delta - \delta^*) \tag{46}$$

$$I = \int_0^\delta \rho u^2 dy = \rho_e u_e^2 (\delta - \delta^* - \theta^*) \tag{47}$$

$$\tilde{J} = \int_0^\delta \rho u H \, dy = \frac{H_e - H_w}{u_e} I + H_w \tilde{m} \tag{48}$$

where equation (42) has been employed in equation (48). From the mass and momentum fluxes, mean velocity $\tilde{u}$ within the viscous layer may be defined as

$$\tilde{u} = \frac{I}{\tilde{m}} = \frac{u_e(\delta - \delta^* - \theta^*)}{\delta - \delta^*} \tag{49}$$

which provides an important parameter

$$\kappa = \frac{\tilde{u}}{u_e} = \frac{\delta - \delta^* - \theta}{\delta - \delta^*} \tag{50}$$

Crocco and Lees (ref. 16) proposed this parameter as the characteristic one with which any state of the viscous layer can be predicted as a single-parameter family. In the present approach, the same physical concept as that of Crocco and Lees is to be given to this parameter on the basis of the assumption mentioned in the preceding section. A mean density $\tilde{\rho}$ and a mean temperature $\tilde{T}$ within the boundary layer can be defined by use of δ and $\tilde{u}$ together with the equation of state; that is,

$$\tilde{m} = \tilde{\rho}\tilde{u}\delta = \frac{p\tilde{u}\delta}{R\tilde{T}}$$

Thus, integration of momentum and energy equations across the boundary layer leads to

$$\frac{dI}{dx} = u_e \frac{d\tilde{m}}{dx} - \delta \frac{dp}{dx} - \tau_w \tag{51}$$

$$\frac{d\tilde{J}}{dx} = H_e \frac{d\tilde{m}}{dx} - q_w \tag{52}$$

By use of equation (48), local heat-transfer rate from equation (52) may be expressed as

$$q_w = (H_e - H_w)\left[(1 - \kappa)\frac{d\tilde{m}}{dx} - \tilde{m}\frac{d\kappa}{dx}\right] \tag{53}$$

On the other hand, geometrical definition of δ and θ gives a mass flux relation (see fig. 4)

$$\frac{d\tilde{m}}{dx} = \rho_e u_e\left(\frac{d\delta}{dx} - \theta\right) \tag{54}$$

which may be reexpressed by introducing the concept of a mixing coefficient, originally proposed by Crocco and Lees, as

$$\frac{d\tilde{m}}{dx} = K\rho_e u_e \tag{55}$$

Therefore,

$$\frac{d\delta}{dx} = K + \theta \tag{56}$$

Since the shock wave is assumed to be replaceable by a family of isentropic waves, the pressure in the external flow is given by the Prandtl-Meyer relation:

$$\frac{dp}{p} = \frac{\gamma M_e^2 d\theta}{\sqrt{M_e^2 - 1}} \tag{57}$$

Moreover, it is convenient to introduce several reduced quantities which are defined as

$$\left.\begin{aligned} w &= \frac{u}{a_o} \\ m &= \tilde{m} a_o \\ \phi_e &= \frac{1 - \frac{\gamma - 1}{2} w_e^2}{\gamma w_e} \end{aligned}\right\} \tag{58}$$

By use of these values, equation (57) can be reexpressed as

$$\frac{dp}{p} = -\frac{dw_e}{\phi_e}$$

To evaluate several physical properties of compressible turbulent boundary layers by use of the incompressible data, the Illingworth-Stewartson transformation (ref. 12) is introduced as

$$\rho_o a_o \, d\eta = \rho a_e \, dy$$

$$p_o a_o \, d\xi = p_e a_e \, dx$$

$$\frac{\rho}{\rho_o} u = \psi_y$$

$$\frac{\rho}{\rho_o} v = -\psi_x$$

$$u_i = \psi_\eta$$

$$v_i = -\psi_\xi$$

and provide a useful correlation between compressible and incompressible flows. The results of the transformation may be summarized as follows:

$$\left.\begin{aligned} &\rho_o u_i \, d\eta = \rho u \, dy \\ &\frac{u_i}{a_o} = \frac{u}{a_e} \\ &\frac{u_i}{u_{ie}} = \frac{u}{u_e} \\ &\tau = \frac{p_e T_e}{p_o T_o} \tau_i \end{aligned}\right\} \tag{59}$$

where the subscript o denotes stagnation conditions of the compressible external flow, to which the corresponding incompressible external flow should be referred.

However, it must be noted that there is no rigorous proof for the validity of the Illingworth-Stewartson transformation in the case of a compressible turbulent boundary layer. Because of the almost complete lack of knowledge of compressibility effects on turbulent boundary layers with a pressure gradient, and also because no other method is available for correlating the compressible turbulent boundary-layer flow with incompressible flow, the Illingworth-Stewartson transformation is used.

Several important relations which result from this transformation are summarized as follows:

$$\delta_i - \delta_i^* = \frac{\rho_e a_e}{\rho_o a_o}(\delta - \delta^*)$$

$$\delta_i - \delta_i^* - \theta_i^* = \frac{\rho_e a_e}{\rho_o a_o}(\delta - \delta^* - \theta^*)$$

$$\kappa = \frac{\delta - \delta^* - \theta^*}{\delta - \delta^*} = \frac{\delta_i - \delta_i^* - \theta_i^*}{\delta_i - \delta_i^*} = \kappa_i$$

$$\tilde{m} = \rho_e u_e(\delta - \delta^*) = \rho_o u_{ie}(\delta_i - \delta_i^*) = \tilde{m}_i$$

where the subscript i denotes corresponding incompressible conditions. The thickness of the boundary layer δ is obtained by

$$\delta = \int_0^{\delta} dy = \frac{\rho_o a_o}{\rho_e a_e} \frac{T_o}{T_e} \int_0^{\delta_i} \frac{T}{T_o} \, d\eta$$

If local stagnation temperature in the viscous layer is denoted by T_s, then

$$\frac{T_s}{T} = 1 + \frac{\gamma - 1}{2} M^2 = 1 + \frac{\gamma - 1}{2} \frac{u^2}{a_o^2} \frac{a_o^2}{a_s^2} \frac{T_s}{T} = 1 + \frac{\gamma - 1}{2} w^2 \frac{H_e}{H} \frac{T_s}{T}$$

and therefore,

$$\frac{T}{T_o} = \frac{T}{T_s}\frac{T_s}{T_o} = \frac{H}{H_e} - \frac{\gamma - 1}{2} w^2$$

which can be reexpressed by use of equation (42) as

$$\frac{T}{T_o} = \lambda + (1 - \lambda)\frac{u}{u_e} - \frac{\gamma - 1}{2} w_e^2 \left(\frac{u}{u_e}\right)^2$$

With the aid of equation (59), the local thickness of the compressible boundary layer is written as

$$\delta = \frac{\rho_o a_o}{\rho_e a_e}\frac{T_o}{T_e}\left[\delta_i - (1 - \lambda)\delta_i^* - \frac{\gamma - 1}{2} w_e^2 \left(\delta_i - \delta_i^* - \theta_i^*\right)\right]$$

where

$$\lambda = \frac{H_w}{H_e}$$

With this value, the mean temperature may be obtained in a form

$$\frac{\tilde{T}}{T_o} = \frac{T_e}{T_o}\frac{\tilde{T}}{T_e} = \kappa^2\left[F_1 - (1 - \lambda) F_2 + 1 - \frac{\gamma - 1}{2} w_e^2\right]$$

where

$$F_1 = \frac{\delta_i^* + \theta_i^*}{\delta_i - \delta_i^* - \theta_i^*}$$

$$F_2 = \frac{\delta_i^*}{\delta_i - \delta_i^* - \theta_i^*}$$

Thus, the mass flux relation (eqs. (58)) is reduced to

$$m\kappa\left[F_1 - (1 - \lambda) F_2 + 1 - \frac{\gamma - 1}{2} w_e^2\right] = \gamma p w_e \delta \tag{60}$$

Differentiation of equation (60) with respect to x and elimination of $d\delta/dx$ by use of equation (56) leads to

$$\left\{\left[\kappa \frac{dF_1}{d\kappa} - \kappa(1 - \lambda)\frac{dF_2}{d\kappa} + P\right]\frac{d\kappa}{dw_e} - (\gamma - 1)\kappa w_e - \frac{\kappa P}{w_e}\right.$$

$$\left. + \frac{\kappa P}{\phi_e}\right\}\frac{dw_e}{d \log m} = \gamma w_e \phi_e\left(1 + \frac{\theta}{K}\right) - \kappa P \tag{61}$$

where

$$P = F_1 - (1 - \lambda) F_2 + 1 - \frac{\gamma - 1}{2} w_e^2 \tag{62}$$

On the other hand, with the aid of equation (49), the momentum equation (eq. (51)) may be reduced to

$$\left(w_e \frac{d\kappa}{dw_e} + \kappa - \frac{\kappa P}{\gamma w_e \phi_e}\right) \frac{dw_e}{d \log m} = w_e(1 - \kappa)(1 - \phi) \tag{63}$$

where

$$\left.\begin{aligned} \phi &= \frac{C_f}{2K(1 - \kappa)} \\ C_f &= \frac{\tau_w}{\frac{1}{2}\rho_e u_e^2} \end{aligned}\right\} \tag{64}$$

Elimination of $dw_e/d(\log m)$ from equations (61) and (63) yields for $\phi \neq 1$

$$\frac{d\kappa}{dw_e} = \frac{B}{A} \tag{65}$$

where

$$A = w_e\left(1 - \frac{\gamma - 1}{2} w_e^2\right)\left\{\left(1 - \frac{\gamma - 1}{2} w_e^2\right)\frac{\theta}{K} + \phi(1 - \kappa)\left(1 - \frac{\gamma - 1}{2} w_e^2\right)\right.$$

$$\left. - \left[F_1 - (1 - \lambda)F_2\right](1 - \phi + \kappa\phi) - \kappa(1 - \kappa)(1 - \phi)\left[\frac{dF_1}{d\kappa} - (1 - \lambda)\frac{dF_2}{d\kappa}\right]\right\}$$

$$B = \kappa(1 - \kappa)(1 - \phi)\left(1 - \frac{\gamma - 1}{2} w_e^2\right)\left(\frac{\gamma + 1}{2} w_e^2 - 1\right) + \kappa\left[F_1 - (1 - \lambda)F_2\right]$$

$$\times \left\{\gamma w_e^2(1 - \kappa)(1 - \phi) + \phi(1 - \kappa)\left(1 - \frac{\gamma - 1}{2} w_e^2\right)\right.$$

$$\left. + \left(1 - \frac{\gamma - 1}{2} w_e^2\right)\frac{\theta}{K} - \kappa\left[F_1 - (1 - \lambda)F_2\right]\right\}$$

Equation (65) is a fundamental equation associated with the rate of change in the state of the internal viscous layer with external conditions. As is seen in the equation, the essential characteristic of the interaction phenomenon is nonlinear. If ϕ is equal to unity, the equation can be reduced to a simple form,

$$\frac{d\kappa}{dw_e} = \frac{\kappa\left[F_1 - (1 - \lambda)F_2\right]}{w_e\left(1 - \frac{\gamma - 1}{2} w_e^2\right)} \tag{66}$$

which is independent of mixing coefficient.

Crocco and Lees (ref. 16) gave a detailed discussion on the solution of equation (65) in the case where $\lambda = 1.0$ and $\phi = 0$ and pointed out the existence of a singular point which is a saddle point of the solution from a mathematical viewpoint. Physically speaking, this singular point corresponds to the sonic point of a convergent-divergent nozzle. However, if ϕ is equal to unity, the singular point vanishes, as is seen in equation (66).

Evaluation of F_1 and F_2 is of interest. Crocco and Lees used an empirical relation for F_1, obtained from the data given by reference 18. However, in the present approach, F_1 and F_2 are estimated from approximate analytical results obtained for the fully developed turbulent boundary layer on a flat plate. If a velocity profile for an incompressible turbulent boundary layer with zero pressure gradient is assumed to be given by a power-law distribution such as

$$\frac{u_i}{u_{ie}} = \left(\frac{y}{\delta_i}\right)^{1/n}$$

then, the displacement thickness and the momentum thickness are obtained, respectively, as

$$\frac{\delta_i^*}{\delta_i} = \frac{1}{1 + n}$$

$$\frac{\theta_i^*}{\delta_i} = \frac{n}{(1 + n)(2 + n)}$$

where n indicates a positive constant. For the flat plate, it is usually assumed that $n = 7$. With these expressions, κ, F_1, and F_2 are given in forms:

$$\left.\begin{aligned} \kappa &= \frac{n + 1}{n + 2} \\ F_1 &= \frac{2}{n} \\ F_2 &= \frac{2 + n}{n(1 + n)} \end{aligned}\right\} \tag{67}$$

Therefore, elimination of n from these equations leads to

$$\left.\begin{aligned} F_1 &= \frac{2(1-\kappa)}{2\kappa - 1} \\ F_2 &= \frac{1-\kappa}{\kappa(2\kappa - 1)} \end{aligned}\right\} \tag{68}$$

Although equations (68) were derived from a relation available for a flat plate, it is capable of representing a universal relation associated with the general state of the incompressible turbulent boundary layer, as long as the assumption of a one-parameter family of boundary-layer state is valid. The reason for this statement is as follows: From the assumption of a one-parameter family for the boundary-layer state, it is recognized that there should exist a unique relation between F_1 and κ which can predict any state of the boundary layer. In other words, F_1 should be a function of κ only. Since flat-plate flow having $\kappa = \kappa_p$ and $F_1 = F_{1p}$ for a specified value of n must be one of the general states, these values have to coincide with those of the unique solution. This condition, in turn, means that the parameter n in equations (67) may be regarded as a parametric variable indicating various states of the boundary-layer flow. Therefore, equations (68) which are obtained by eliminating the parametric variable can be regarded as a representative form of the unique relation between F_1 and κ. The same reasoning is true for F_2.

Evaluation of ϕ in equation (64) is another point of interest. From equations (59) it is easily shown that

$$C_f = \frac{p_e \rho_o}{p_o \rho_e} \frac{a_e^2}{a_o^2} \left(\frac{u_{ie}}{u_e}\right)^2 C_{f,i} = \frac{p_e \rho_o}{p_o \rho_e} C_{f,i}$$

On the other hand, from the definition of the mixing coefficient

$$\frac{d\tilde{m}}{dx} = K\rho_e u_e = \frac{d\tilde{m}_i}{d\xi} \frac{d\xi}{dx} = K_i \rho_o u_{ie} \frac{p_e a_e}{p_o a_o}$$

Therefore,

$$K = \frac{p_e \rho_o}{p_o \rho_e} K_i \tag{69}$$

and

$$\phi = \frac{C_f}{2K(1-\kappa)} = \frac{C_{f,i}}{2K_i(1-\kappa_i)} = \phi_i \tag{70}$$

Equation (70) clearly indicates that ϕ does not change through the Illingworth-Stewartson transformation. For the flat-plate flow, the incompressible mass flux is given by

$$\tilde{m}_i = \rho_o u_{ie}\left(\delta_i - \delta_i^*\right) = \rho_o u_{ie} \frac{n}{1+n} \delta_i$$

Differentiation of $\tilde{m}_i$ with respect to ξ leads to

$$K_i = \frac{n}{1+n} \frac{d\delta_i}{d\xi} \tag{71}$$

On the other hand, the skin-friction coefficient is given by

$$C_{f,i} = 2 \frac{d\theta_i^*}{d\xi} = \frac{2n}{(1+n)(2+n)} \frac{d\delta_i}{d\xi}$$

Hence,

$$\frac{C_{f,i}}{2K_i} = \frac{1}{2+n} = 1 - \kappa_i$$

and

$$\phi_{i,p} = 1$$

for a flat plate. Unfortunately, for general states of boundary-layer flow other than the flat plate, there does not exist any rigorous theory for evaluating ϕ_i. Moreover, even the empirical information is meager. For this reason, it is assumed in the present analysis that ϕ is equal to unity everywhere in the recompression region.

The value of the mixing coefficient remains to be discussed. The mixing coefficient of a compressible family is correlated with that of the incompressible one through equation (69). It is easily deduced from equation (71) that the local mixing coefficient for attached boundary-layer flow is, in general, a function of the local Reynolds number. However, even if such a formulation had been made, it is still doubtful whether it could give a correct answer that would include the effects of compressibility. When it is considered that the mass-flow variation has only a little effect on the turbulent values and that insufficient empirical data are available on the spread of turbulence, it seems justifiable to introduce the approximation that the mixing coefficient is constant throughout the recompression region.

From the data presented in reference 19, Crocco and Lees estimated that $K = 0.03$ near the separation point of the attached turbulent boundary layer. A rough evaluation of the mixing coefficient by use of equation (29) indicates that $K \approx \frac{0.139}{X}$ in the jet mixing region. Of course, this value may vary depending upon the definition of the upper jet boundary. Nevertheless, it is more than four times the Crocco and Lees' value for $X = 1.0$. On the other hand, the flat-plate value for a Reynolds number of 10^5 indicates that $K \approx 6 \times 10^{-3}$, which is only one-fifth of Crocco and Lees' value. When the fact that the actual value of the mixing coefficient in the recompression region should

vary from $K \approx \frac{0.139}{X}$ at the entrance to $K \approx 6 \times 10^{-3}$ at the exit of this region is considered, the value proposed by Crocco and Lees is realistic as a mean value. Therefore, the mixing coefficient is, for the present, taken as $K = 0.03$, where this value should be regarded as a realistic mean value in the recompression region. However, it should be noted that the value of the mixing coefficient has a strong influence on the thickness of the boundary layer and the associated local heat-transfer rate in the recompression region.

Since the viscous layer downstream of the recompression region has been assumed to be a fully developed turbulent boundary layer on a flat plate, integration of equation (65) is made upstream starting from the exit point of the recompression region with the known value of w_e and κ appropriate to the flat-plate flow conditions. From the assumption of isentropic recompression, the Mach number of the external flow downstream of the recompression region must equal the oncoming value. Therefore the starting values are given by

$$\left.\begin{aligned} (w_e)_{Start} &= w_{e,p} = \frac{M_\infty}{\sqrt{1 + \frac{\gamma - 1}{2} M_\infty^2}} \\ (\kappa)_{Start} &= \kappa_p = \frac{8}{9} \end{aligned}\right\} \tag{72}$$

For the case of $\phi = 1$, equation (66) can be integrated analytically in a form

$$(1 - \kappa)^{\frac{1}{1+\lambda}} (2\kappa - 1 + \lambda)^{\frac{\lambda}{1+\lambda}} = \tilde{C} \frac{\sqrt{1 - \frac{\gamma - 1}{2} w_e^2}}{w_e} \tag{73}$$

where $\tilde{C}$ is an integral constant to be determined from equations (72).

Other Relations Associated With Recompression Region

Since the solution of the fundamental equation (eq. (65) or eq. (66)) has been obtained, other quantities concerning the recompression region can be estimated. For this purpose it will be convenient to introduce nondimensional quantities defined as

$$\left.\begin{aligned} \bar{m} &= \frac{m}{m_p} \\ \bar{\delta} &= \frac{\delta}{\delta_p} \\ \bar{x} &= -\frac{x}{\delta_p} \end{aligned}\right\} \tag{74}$$

where the subscript p denotes conditions at the exit of the recompression region and the origin of the x-axis has been taken at the exit point.

The equation for mass flux is given from equation (63) for $\phi \neq 1$ as

$$\frac{d\overline{m}}{dw_e} = \frac{\overline{m}}{w_e(1-\kappa)(1-\phi)}\left\{w_e \frac{d\kappa}{dw_e} - \frac{\kappa\left[F_1 - (1-\lambda)F_2\right]}{\gamma w_e \phi_e}\right\} \tag{75}$$

In the case $\phi = 1$, this equation may be reduced to

$$\frac{d\overline{m}}{dw_e} = \frac{\overline{m}E_2}{E_1} \tag{76}$$

where

$$E_1 = \left(1 + \frac{\theta}{K}\right)\left(1 - \frac{\gamma - 1}{2} w_e^2\right) - \kappa P$$

$$E_2 = \left[\kappa \frac{dF_1}{d\kappa} - \kappa(1-\lambda)\frac{dF_2}{d\kappa} + P\right]\frac{d\kappa}{dw_e} + \kappa P\left(\frac{1}{\phi_e} - \frac{1}{w_e}\right) - (\gamma - 1)\kappa w_e$$

and where P has been given by equation (62). The boundary condition is given by

$$\overline{m} = 1 \qquad \left(w_e = w_{e,p}\right) \tag{77}$$

By use of the mass flux $\overline{m}_r$ thus obtained at the entrance of recompression region, the value of ζ_i, which was unknown in the earlier development, can be determined through continuity of mass flux between the jet mixing region and the recompression region. From equation (60), there results

$$\left(\frac{\delta}{\overline{m}}\right)_r = \frac{\kappa_r P_r}{\gamma p_1 w_{e1}} \tag{78}$$

where the subscript r denotes conditions at the entrance of the recompression region (or exit of the jet mixing region). On the other hand, the mass flux at the exit of the jet mixing region has been given by equation (28), and the thickness of the mixing layer at the same station is given by the equation

$$\delta_r = \int_{y_i}^{y_u} dy = \frac{L}{\sigma_1 \sqrt{N_{Re,L}}} \int_{\zeta_i}^{\zeta_u} \frac{h^*}{u^*} d\zeta$$

Therefore,

$$\left(\frac{\delta}{\overline{m}}\right)_r = \left(\frac{\delta}{\tilde{m} a_o}\right)_r = \frac{J(\zeta_u) - J(\zeta_i)}{\rho_1 u_1 a_o(\zeta_u - \zeta_i)} \tag{79}$$

Thus, from equations (78) and (79), the following relation which determines ζ_i uniquely is obtained:

$$\frac{J(\zeta_u) - J(\zeta_i)}{\zeta_u - \zeta_i} = \frac{\kappa_r\left[F_{1,r} - (1 - \lambda)F_{2,r} + 1 - \frac{\gamma - 1}{2} w_{e,1}^2\right]}{1 - \frac{\gamma - 1}{2} w_{e,1}^2} \tag{80}$$

Thickness of the boundary layer is estimated from equation (60); that is,

$$\bar{\delta} = \frac{\delta}{\delta_p} = \frac{p_p}{p} \frac{w_{e,p}}{w_e} \frac{\kappa}{\kappa_p} \frac{P}{P_p} \bar{m}$$

which is further rewritten by use of isentropic relations in a form

$$\bar{\delta} = \frac{w_{e,p}}{w_e}\left(\frac{1 - \frac{\gamma - 1}{2} w_{e,p}^2}{1 - \frac{\gamma - 1}{2} w_e^2}\right)^{\frac{\gamma}{\gamma - 1}} \frac{\kappa}{\kappa_p} \frac{P}{P_p} \bar{m} \tag{81}$$

The equation for the width of the recompression region can be obtained from the definition of the mixing coefficient. Rewriting equation (55) yields

$$\frac{d\bar{m}}{d\bar{x}} = -\frac{\delta_p}{m_p} \rho_e u_e a_o K$$

which can be reexpressed, with the aid of equation (60), as

$$\frac{d\bar{x}}{dw_e} = -\frac{w_{e,p}}{K\kappa_p P_p} \frac{1 - \frac{\gamma - 1}{2} w_e^2}{w_e}\left(\frac{1 - \frac{\gamma - 1}{2} w_{e,p}^2}{1 - \frac{\gamma - 1}{2} w_e^2}\right)^{\frac{\gamma}{\gamma - 1}} \frac{d\bar{m}}{dw_e} \tag{82}$$

where the boundary condition is given as

$$\bar{x} = 0 \qquad (w_e = w_{e,p}) \tag{83}$$

The local heat-transfer rate can be obtained from equation (53) as

$$\frac{q_w}{\rho_\infty u_\infty (H_e - H_w)} = \frac{1 - \frac{\gamma - 1}{2} w_{e,p}^2}{\kappa_p P_p}\left[\bar{m} \frac{d\kappa}{dw_e} - (1 - \kappa) \frac{d\bar{m}}{dw_e}\right] \frac{dw_e}{d\bar{x}} \tag{84}$$

The mean heat-transfer rate $\tilde{q}_R$ in the recompression region is defined by the equation

$$\tilde{q}_R = \frac{1}{-x_r} \int_{x_r}^{0} q_w \, dx$$

where the negative sign of x_r is due to the coordinates system used for the recompression region. (See fig. 4.) By use of nondimensional expressions, the preceding equation can be reduced to

$$\frac{\tilde{q}_R}{\rho_\infty u_\infty (H_e - H_w)} = \frac{1}{\bar{x}_r} \int_{w_{e,p}}^{w_{e,1}} C_{q,R} \frac{d\bar{x}}{dw_e} dw_e \tag{85}$$

where

$$C_{q,R} = \frac{q_w}{\rho_\infty u_\infty (H_e - H_w)}$$

which has already been given by equation (84). The mean heat-transfer coefficient in the recompression region $\tilde{C}_{q,R}$ is defined by the equation

$$\tilde{C}_{q,R} = \frac{\tilde{q}_R}{\rho_\infty u_\infty H_\infty}$$

HEAT-TRANSFER REDUCTION IN THE REGION DOWNSTREAM OF RECOMPRESSION

Since the coolant flow is assumed to be injected into the dead-air region at a low flow rate through a rearward-facing slot, complete mixing occurs between the coolant and the oncoming viscous flow before the exit of the recompression region is approached so that the viscous layer downstream of the recompression region is an ordinary turbulent boundary layer on a flat plate (fig. 5). Therefore, the predominant factor in reducing the heat-transfer rate in this region will be the growth of boundary-layer thickness.

Since the recompression has been assumed to be made through a family of isentropic compression waves, the Mach number of the external flow must be the oncoming value. In contrast to the jet mixing region upstream, this characteristic makes the subsequent analysis fairly simple because the external flow Mach number remains unchanged with coolant flow rate.

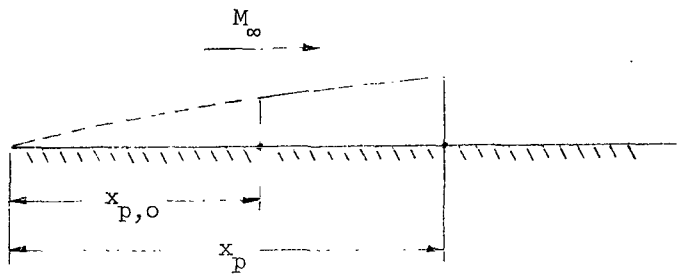

Figure 5.- Basic turbulent boundary layer along an infinite flat plate.

For fully developed compressible turbulent boundary-layer flows without pressure gradient (flat plate), Van Driest (ref. 17) presented an analytical approach whose results are shown to be in good agreement with existing experimental data. Therefore, subsequent development will use the analytical results presented by Van Driest. It must be noted that although coolant flow rate does not appear explicitly in the subsequent analysis, its effect is implicitly involved in the development because the behavior of the attached boundary layer is seriously influenced by the upstream conditions.

The local skin-friction coefficient $C_{f,\infty}$ and the energy transfer coefficient $C_{H,\infty}$ obtained by Van Driest for a fully developed turbulent boundary layer on a flat plate may be summarized as follows:

$$\frac{0.242}{N_1 C_{f,\infty}^{1/2}}\left(\frac{T_\infty}{T_w}\right)^{1/2}\left(\sin^{-1}\alpha + \sin^{-1}\beta\right) = \log_{10} N_{Re,\infty} C_{f,\infty} - \frac{1 + 2\omega}{2}\log_{10}\frac{T_w}{T_\infty} + 0.41 \tag{86}$$

and

$$C_{H,\infty} = \frac{\bar{q}_w}{\rho_\infty u_\infty (H_\infty - H_w)} = \frac{1}{2} C_{f,\infty} \tag{87}$$

where

$$C_{f,\infty} = \frac{\tau_w}{\frac{1}{2}\rho_\infty u_\infty^2} \tag{88}$$

$$N_{Re,\infty} = \frac{u_\infty x}{\nu_\infty} \tag{89}$$

$$\left.\begin{aligned} N_1 &= \sqrt{\frac{\gamma - 1}{2} M_\infty^2 \frac{T_\infty}{T_w}} \\ N_2 &= \left(1 + \frac{\gamma - 1}{2} M_\infty^2\right)\frac{T_\infty}{T_w} - 1 \\ \alpha &= \frac{2N_1^2 - N_2}{\sqrt{N_2^2 + 4N_1^2}} \\ \beta &= \frac{N_2}{\sqrt{N_2^2 + 4N_1^2}} \end{aligned}\right\} \tag{90}$$

and where x denotes a distance measured from leading edge of the flat plate where the thickness of the boundary layer is zero. It should be noted that these relations are obtained under the assumption of a turbulent Prandtl number equal to unity. Thus, the local thickness of the boundary layer is given by

$$\delta = \frac{\tilde{K}\left(1 + N_2 - N_1^2\right)^{1/2}}{\sqrt{2}} \left(\frac{T_w}{T_\infty}\right)^{1/2} C_{f,\infty}{}^{1/2} x \tag{91}$$

where

$$\tilde{K} = \frac{1}{4.15\sqrt{2}\,\log_{10} e} \tag{92}$$

Therefore, equation (91) can be simplified, by use of equation (90), to a form

$$\delta = \frac{1}{3.6} x C_{f,\infty}{}^{1/2} \tag{93}$$

On the other hand, from equations (86) and (89), a relation between the local skin-friction coefficient and x can be obtained as

$$N_{Re,\infty} = \frac{u_\infty x}{\nu_\infty} = \left(\frac{T_w}{T_\infty}\right)^{\frac{1+2\omega}{2}} \frac{1}{C_{f,\infty}} \exp\left[\frac{0.557}{N_1 C_{f,\infty}{}^{1/2}} \left(\frac{T_\infty}{T_w}\right)^{1/2} \left(\sin^{-1}\alpha + \sin^{-1}\beta\right) - 0.944\right] \tag{94}$$

Substitution of equation (93) into equation (94) and elimination of x then leads to

$$\left(\frac{T_w}{T_\infty}\right)^{\frac{1+2\omega}{2}} \frac{1}{\sqrt{C_{f,\infty}}} \exp\left[\frac{0.557}{N_1 \sqrt{C_{f,\infty}}} \left(\frac{T_\infty}{T_w}\right)^{1/2} \left(\sin^{-1}\alpha + \sin^{-1}\beta\right) - 0.944\right] = 3.6\, N_{Re,D} \frac{L}{D} \frac{\delta}{L} \tag{95}$$

where

$$N_{Re,D} = \frac{u_\infty D}{\nu_\infty} \tag{96}$$

Thus, if the Mach number of the external flow M_∞ and the temperature ratio T_w/T_∞ are given, solutions for the basic turbulent boundary-layer flow (Van Driest's solution) become known in detail.

For the present problem, a fully developed turbulent boundary layer has been assumed to develop downstream starting from the exit of the recompression region with a finite thickness δ_p. Based on the discussion in the previous paragraphs, it seems

reasonable to assume that characteristics of the actual boundary layer are the same as those of the basic boundary-layer flow, in the region downstream of a point where the thickness of the basic boundary layer is equal to δ_p. Furthermore, δ_p/L is known from the solutions of the jet mixing region and recompression region to be

$$\frac{\delta_p}{L} = \frac{1}{\bar{\delta}_r}\frac{\delta_r}{L}$$

Therefore, the corresponding station x_p and the skin-friction coefficient $C_{f,\infty,p}$ in the basic boundary layer are found from equations (93) and (95) to be

$$\left(\frac{T_w}{T_\infty}\right)^{\frac{1+2\omega}{2}} \frac{1}{\sqrt{C_{f,\infty,p}}} \exp\left[\frac{0.557}{N_1\sqrt{C_{f,\infty,p}}}\left(\frac{T_\infty}{T_w}\right)^{1/2}\left(\sin^{-1}\alpha + \sin^{-1}\beta\right) - 0.944\right] = 3.6\,\frac{N_{Re,D}}{\bar{\delta}_r}\frac{L}{D}\frac{\delta_r}{L} \tag{97}$$

$$x_p^* = \frac{x_p}{L} = \frac{3.6}{\sqrt{C_{f,\infty,p}}}\frac{\delta_r}{L} \tag{98}$$

where

$$\frac{T_w}{T_\infty} = \left(1 + \frac{\gamma - 1}{2} M_\infty^2\right)\frac{H_w}{H_\infty} \tag{99}$$

If the coolant flow rate increases, the other oncoming flow conditions remaining unchanged, δ_p will increase because of the increase of mass flux across the boundary layer. This increase, in turn, tends to shift the starting point of the actual boundary layer downstream when it is transferred to the basic boundary-layer contour. (See fig. 5.) This statement follows, since, as is seen in equations (97) and (98), the increase in δ_r results in a decrease in $C_{f,\infty,p}$ and, consequently, an increase in x_p^*. Moreover, since the skin-friction coefficient decreases, the surface heat input will to a certain extent decrease.

In order to examine this effect more quantitatively, the local effectiveness of coolant injection η_f associated with the fully developed turbulent boundary-layer region is defined as

$$\eta_f = \frac{\int_{x_{p,o}}^{\infty} q_{w,o}\,dx - \int_{x_p}^{\infty} q_w\,dx}{\rho_c u_c H_\infty D} \tag{100}$$

Since the local heat-transfer rate $\bar{q}_w(x)$ associated with the basic boundary-layer flow is kept unchanged irrespective of the coolant flow rate, the numerator on the right-hand side of equation (100) may be evaluated as

$$\int_{x_{p,o}}^{\infty} q_{w,o}\,dx - \int_{x_p}^{\infty} q_w\,dx = \int_{x_{p,o}}^{x_p} \bar{q}_w(x)\,dx$$

where $\bar{q}_w(x)$ has been given by equation (87) and the subscript o denotes the no-coolant-flow condition. Thus, by introducing nondimensional expressions and replacing x by $C_{f,\infty}$ as an integral variable, equation (100) may be reduced to

$$\eta_f = \frac{1}{2}\left(1 - \frac{H_w}{H_\infty}\right)\frac{1}{N_{Re,D}\dot{M}}\int_{C_{f,\infty,p_o}}^{C_{f,\infty,p}} C_{f,\infty}\,\frac{dN_{Re,\infty}}{dC_{f,\infty}}\,dC_{f,\infty} \tag{101}$$

where

$$\frac{dN_{Re,\infty}}{dC_{f,\infty}} = -\left(\frac{T_w}{T_\infty}\right)^{\frac{1+2\omega}{2}}\frac{1}{C_{f,\infty}^{\,2}}\left[1 + \frac{0.557}{2N_1\sqrt{C_{f,\infty}}}\left(\frac{T_\infty}{T_w}\right)^{1/2}\left(\sin^{-1}\alpha + \sin^{-1}\beta\right)\right]$$

$$\times \exp\left[\frac{0.557}{N_1\sqrt{C_{f,\infty}}}\left(\frac{T_\infty}{T_w}\right)^{1/2}\left(\sin^{-1}\alpha + \sin^{-1}\beta\right) - 0.944\right] \tag{102}$$

The overall effectiveness of coolant injection η_T may be defined by an equation

$$\eta_T = \frac{\int_0^{\infty}\left(q_{w,o} - q_w\right)dx}{\rho_c u_c H_\infty D} \tag{103}$$

where the origin of the x-axis is taken at the slot exit and q_w denotes local heat-transfer rate to the wall. Equation (103) can be reexpressed as

$$\eta_T = \frac{\left(\tilde{C}_{q,j,o} - \tilde{C}_{q,j}\right)L}{\dot{M}D} + \frac{\left(\tilde{C}_{q,R,o} - \tilde{C}_{q,R}\right)L}{\dot{M}D} + \eta_f - \tilde{C}_{q,j,o}\,\frac{L - L_o}{\dot{M}D} + \tilde{C}_{q,R,o}\,\frac{l_o - l}{\dot{M}D}$$

where L and l denote the length of the jet-mixing and recompression regions, respectively, and the subscript o indicates the no-coolant-flow condition, and where subscripts j, R, and f denote conditions in regions of jet mixing, recompression, and fully developed turbulent boundary layer, respectively.

RESULTS AND DISCUSSION

Jet Mixing Region

Numerical calculations for determination of the flow field in the jet mixing region can be carried out by the following procedure. First, the Mach number of the oncoming flow M_∞, the ratio of wall enthalpy to stagnation enthalpy of oncoming flow H_w/H_∞, and the ratio of stagnation enthalpy of coolant flow to wall enthalpy H_c/H_w are specified, and a flow deflection angle θ of the external isentropic flow through a Prandtl-Meyer fan is assumed. These values permit calculation of the Mach number of the external flow M_1 in the jet mixing region, and also determination of the shock-wave strength in the recompression region. It must be noted that the assumption of θ specifies the pressure p_1 in the jet mixing region. Since the strength of the shock wave is known, any solution associated with the recompression region can be considered to have already been determined at this stage of calculation.

Since M_1 is known, velocity and enthalpy profiles are calculated from equations (16) and (17), respectively. These profiles, in turn, permit determination of ζ_i by use of equation (80). If u_c^* is assumed to be zero (no coolant flow) at this flow deflection angle, then the parameter Z becomes known from equations (24) and (25), because $\zeta_d = \zeta_i$. Thus, by changing the value of θ (or M_1) but keeping $u_c^* = 0$, a relation between p_1 and $Z \left(= \frac{C}{D \sqrt[n]{N_{Re}}}\right)$ can be obtained. This relation indicates the usual base pressure associated with a rearward-facing step, which should be the minimum value of pressure in the jet mixing region for the case of film cooling. Since oncoming flow conditions and slot geometry have been given or are known a priori, the value of Z is known and, consequently, θ or p_1 is known from the relation just obtained. The data (M_o, p_o, Z) thus obtained for the no-coolant-flow case are considered to be starting conditions for the coolant-flow case.

In the case of coolant mass injection, essentially the same procedure as used for the no-coolant-flow case is applied to obtain ζ_d, except that Z is kept constant irrespective of coolant flow rate, since the oncoming flow is not influenced by the coolant mass injection. For this purpose, a new flow deflection angle θ, smaller than θ_o, is specified and the coolant flow velocity is assumed. However, at this stage of calculation, it is not yet known whether the assumed value of u_c^* is compatible with the specified value of θ or M_1.

Since H_c/H_∞ has been specified, it is easily shown from isentropic relations that the static enthalpy of coolant at the slot exit is given by the equation

$$h_c^* = \left(1 + \frac{\gamma - 1}{2} M_1^2\right)\frac{H_c}{H_\infty} - \frac{\gamma - 1}{2} M_1^2 u_c^{*2} \tag{104}$$

Therefore, an assumed local coolant flow rate can be obtained from the assumed value of u_c^* through the equation

$$\rho_c^* u_c^* = \frac{u_c^*}{h_c^*} \tag{105}$$

Moreover, δ_1^*/D and θ_1^*/D are obtained from equations (26) so that ζ_d and $J(\zeta_m)$ are known from equations (23) and (25).

Once ζ_d and $J(\zeta_m)$ have been determined in this way, the length of the mixing region L/D is known from equation (21) and, consequently, $\rho_c^* u_c^*$ can be evaluated again from equation (19). However, this resultant coolant flow rate does not always coincide with the value initially assumed because, physically speaking, the solution to u_c^* must be unique for a specified value of θ. Therefore, it is necessary to repeat the calculation, the assumed value of u_c^* being adjusted, until the resultant coolant flow rate coincides with the assumed one. The coolant flow velocity and coolant flow rate obtained in this way are unique for the specified values of θ and Z.

Figure 6 shows a typical example of velocity and enthalpy profiles across the mixing layer for $M_\infty = 3.0$, $\theta = 9^o$ $(M_1 = 3.514)$, and $H_w/H_\infty = 0.3571$. Figure 7 presents the variation of pressure in the jet mixing region with Z for $M_\infty = 2.0$, $H_w/H_\infty = 1.0$ and $u_c^* = 0$, where the oncoming boundary layer is assumed to be laminar ($n = 2$). In the figure are also plotted the experimental results obtained by Chapman, Wimbrow, and Kester (ref. 15) for $M_\infty = 2$. However, since the value of $\tilde{\phi}_j$ expressed by equation (31) has been determined to obtain good agreement of base pressure between the present approach and the data of reference 15 at $M_\infty = 2$, the good agreement indicated in figure 7 should have been a natural result. Because of this circumstance, base pressure has been calculated for $M_\infty = 3$ to confirm the present approach, and the results are shown in figure 8, together with the data of reference 15 for comparison. As is seen in figure 8, agreement between theory and experiment is fairly good; thus, the present approach is confirmed.

Figure 9 shows several examples of pressure variation in the jet mixing region with coolant flow rate, where Z is used as a parameter. The pressure increases with the increase of the coolant flow rate. This characteristic may be understood by the following consideration. If parametric conditions are fixed, it is easily shown that the minimum pressure attainable in the dead-air region is the base pressure corresponding to $u_c^* = 0$, below which fluid in the dead-air region will be sucked into the coolant slot. Therefore, in order that the coolant mass be injected, the pressure of coolant flow at the slot exit must be higher than the base pressure without coolant flow. This condition, in turn, increases the pressure in the dead-air region, since coolant flow is subsonic at the slot

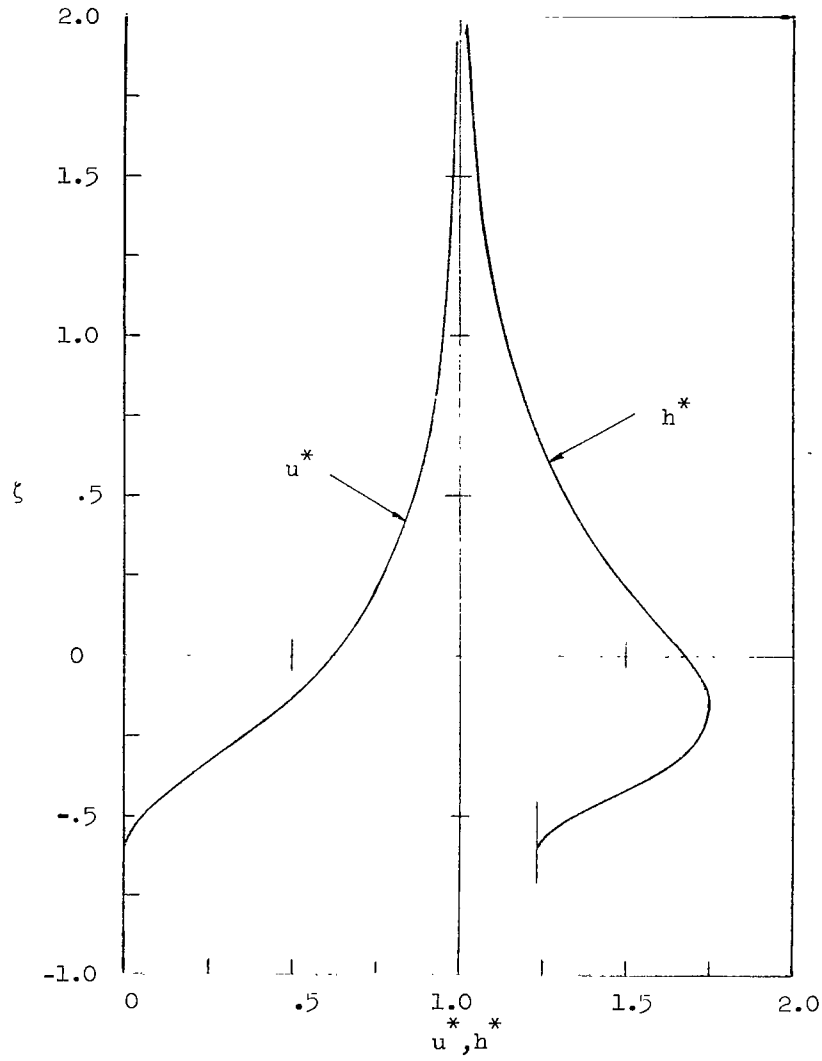

Figure 6.- Velocity and enthalpy profiles across jet mixing layer. $M_1 = 3.514$; $H_w/H_\infty = 0.3571$; $N_{Pr,t} = 1.0$.

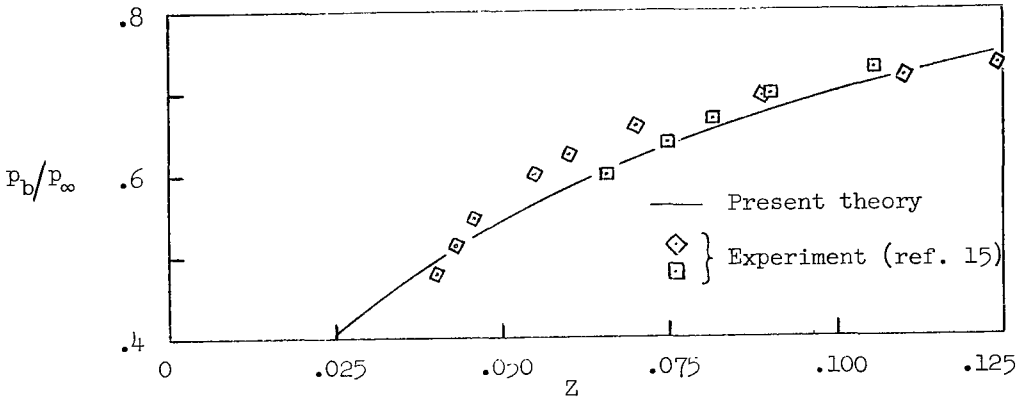

Figure 7.- Base pressure. $M_\infty = 2.0$; $H_w/H_\infty = 1.0$; $N_{Pr,t} = 1.0$; $\dot{M} = 0$.

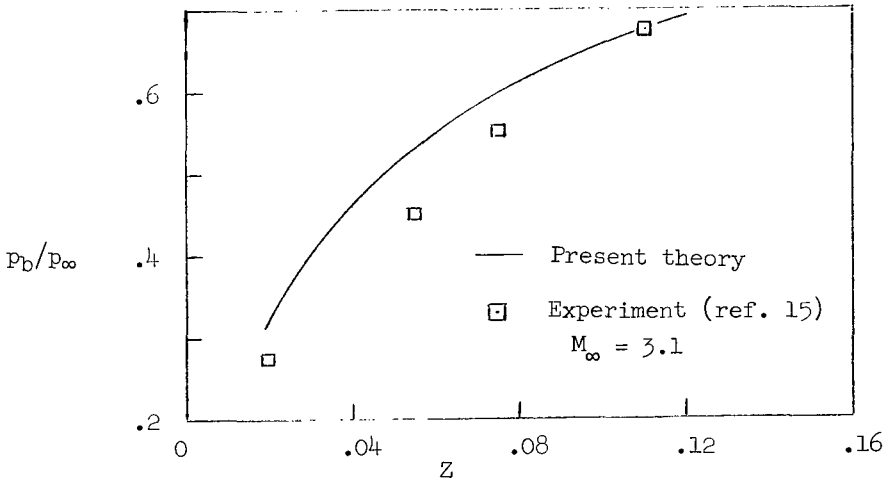

Figure 8.- Base pressure. $M_\infty = 3.0$; $H_w/H_\infty = 1.0$; $N_{Pr,t} = 1.0$; $\dot{M} = 0$.

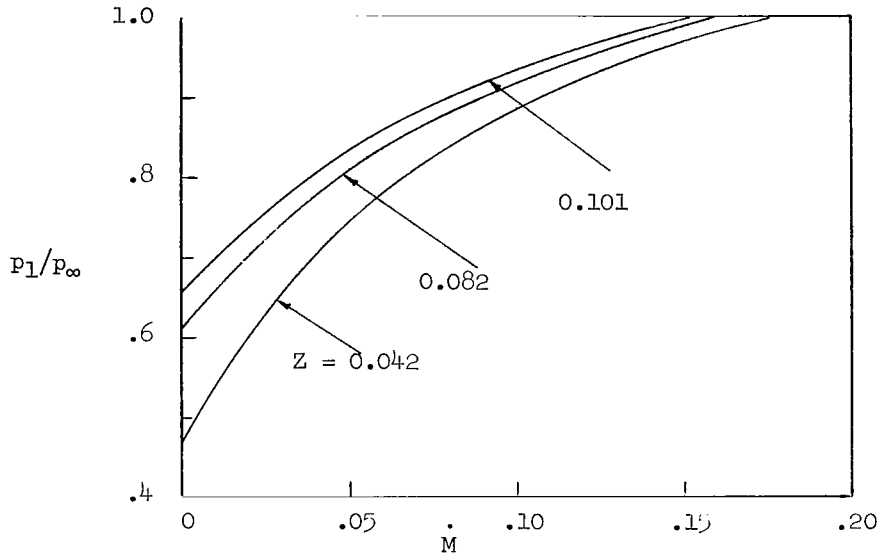

Figure 9.- Variation of pressure in jet mixing region with coolant flow rate. $M_\infty = 3.0$; $H_w/H_\infty = 0.3571$; $H_c/H_w = 1.0$; $N_{Pr,t} = 1.0$.

exit. The increase of dead-air pressure decreases the strength of the Prandtl-Meyer fan. More intuitively, it might be deduced that the separated boundary layer, which acts as though it were an impermeable membrane, is so pushed upward, through a higher pressure inside which is supported by the coolant flow, as to reach a new equilibrium position and, therefore, the flow deflection angle of the external stream decreases to increase the pressure downstream of the Prandtl-Meyer fan.

Figure 10 presents a variation of the length of the separated region (length of mixing region) with coolant flow rate for $M_\infty = 3.0$, $H_w/H_\infty = 1.0$, and $Z = 2.8 \times 10^{-2}$. As is seen in the figure, the length increases with an increase of coolant flow and this characteristic supports the intuitive deduction of a pressure increase, due to the coolant flow, mentioned in the last paragraph.

In order to confirm further the validity of the present approach, an experimental curve for effective length of film cooling obtained by Goldstein, Eckert, Tsou, and Haji-Sheikh (ref. 4) is shown in figure 10 for comparison. However, it must be remarked that there is a difference in the physical meaning of L/D between theory and experiment indicated in figure 10. In the experiment L is defined as the length measured from the slot exit for which the effectiveness of film cooling η_{eff} defined by the equation

$$\eta_{eff} = \frac{T_w - T'_r}{T_{w,2} - T'_{r,2}}$$

is assumed to be kept as unity, where T_w is the adiabatic wall temperature and $T_{w,2}$, its value at the point of injection. Here, T'_r is the wall temperature for isoenergetic

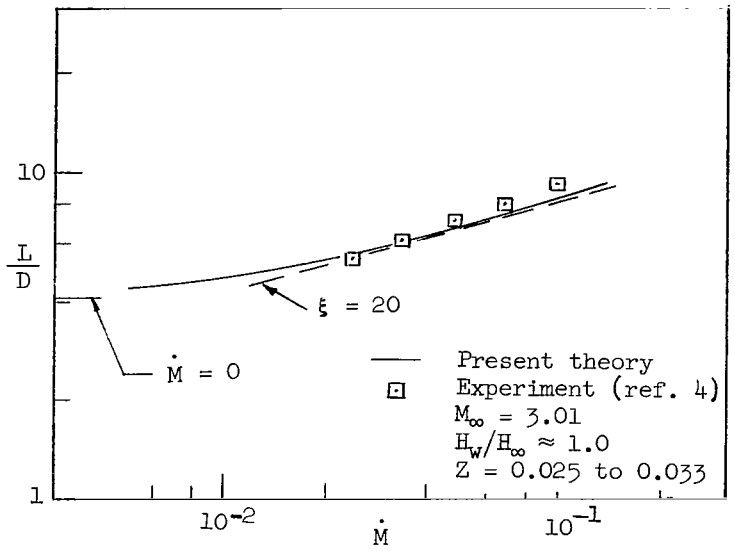

Figure 10.- Length of separated region. $M_\infty = 3.0$; $H_W/H_\infty = 1.0$; $H_C/H_W = 1.0$; $Z = 0.0282$; $X = 1.0$; $N_{Pr,t} = 1.0$.

injection ($H_C = H_\infty$) at the same blowing rate, and $T'_{r,2}$ indicates the value at the point of injection. Thus, the experimental length L/D in figure 10 has the physical meaning that the wall temperature T_W changes abruptly to approach T'_r downstream of the point where $x = L$. However, in spite of the physical meaning of L/D being different between the present theory and the experiment, the comparison shown in figure 10 seems to be reasonable because the change of wall temperature clearly indicates an abrupt change of surface heating rate which will take place at the end of the jet mixing region, because the mixing between oncoming flow and coolant flow has almost finished before the recompression region is approached. This reasoning can be confirmed by observation of schlieren photographs of the shock-wave location presented in reference 4. Thus, the experimental length L/D might be interpreted as the length of separated region.

Goldstein, Eckert, Tsou, and Haji-Sheikh plotted the value of η_{eff} against a parameter $\bar{\xi}$ defined by the equation

$$\bar{\xi} = \frac{L}{D}\left(\frac{1}{\dot{M}}\right)^{0.4}$$

and obtained $\bar{\xi} = 23.5$ for $\eta_{eff} = 1$ by means of extrapolation of the mean data curve in the case of small coolant injection ($\dot{M} \leq 0.12$). However, detailed examination of the experimental data (fig. 4 of ref. 4) clearly reveals that $\bar{\xi} = 23.5$ is too high; the correct value should be near $\bar{\xi} = 20$. Since a choice of $\bar{\xi} = 20$ seems to be more realistic from the experimental viewpoint, an empirical curve defined by the equation

$$\frac{L}{D} = 20\dot{M}^{0.4} \tag{106}$$

is also shown in figure 10 for comparison. As is seen in the figure, agreement between present theory and the empirical data given by equation (106) seems to be fairly good.

Figures 11 and 12 show the effects of Z and wall enthalpy on the length of the separated region. In general, the length of the separated region primarily depends upon the flow deflection angle which the external stream makes with the wall, and this condition leads to the intuitive deduction that the weaker the Prandtl-Meyer expansion at the

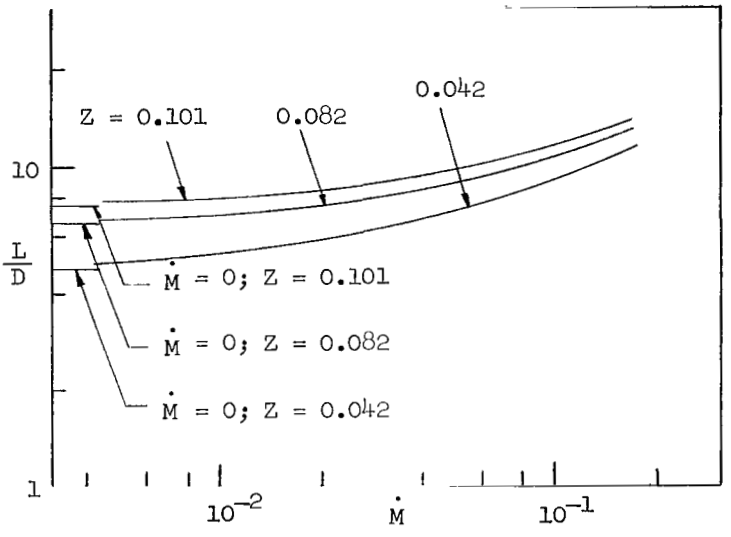

Figure 11.- Length of separated region. $M_\infty = 3.0$; $H_w/H_\infty = 0.3571$; $H_c/H_w = 1.0$; $X = 1.0$; $N_{Pr,t} = 1.0$.

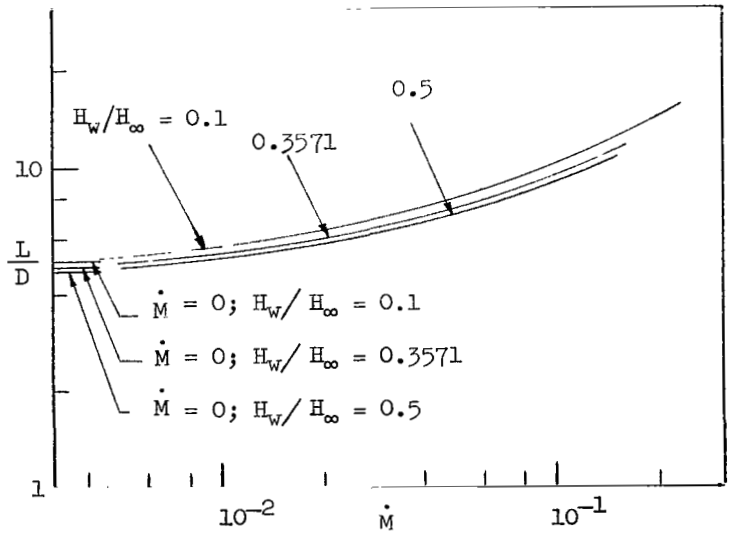

Figure 12.- Length of separated region. $M_\infty = 3.0$; $H_c/H_w = 1.0$; $Z = 0.042$; $X = 1.0$; $N_{Pr,t} = 1.0$.

edge of the plate lip, the longer the separated region becomes. Since the strength of the Prandtl-Meyer fan decreases with the increase of either Z or $\dot{M}$ as is seen in figure 9, the results shown in figure 11 seem to be quite reasonable.

It is generally recognized that the thickness of an attached boundary layer becomes smaller for a lower wall enthalpy. Detailed examination of velocity and enthalpy profiles across the jet mixing region reveals that the same is true for turbulent jet mixing. In fact, the value of the second term on the right-hand side of equation (21) decreases as the wall enthalpy decreases and, consequently, the length of the separated region increases. However, it is easily shown from a comparison of figure 12 with figure 11 that the length of the separated region is less sensitive to wall enthalpy than to the parameter Z. The same trend has already been pointed out experimentally in reference 4 for the case of coolant injection through a rearward-facing slot; thus, further experimental evidence is given of the validity of the present approach.

Figure 13 presents the variation of the mean heat-transfer rate with Z for no coolant flow. It is well-known that the heat-transfer rate for an attached boundary layer depends primarily upon the rate of energy transport into the boundary layer from the external stream, the difference between adiabatic wall temperature and actual wall temperature, and the boundary-layer thickness. Therefore, if the wall temperature and the stagnation enthalpy of the external isentropic stream are assumed to be fixed, then the local heat-transfer rate depends mainly upon the local Mach number of the external stream. This condition follows because the local thickness of the boundary layer and the mixing coefficient in general do not change so abruptly even under the influence of pressure gradient, except for some particular cases such as flow separation. Inasmuch as the local rate of energy transport is proportional to the local mass flow rate of the external flow, which decreases with an increase of local Mach number if the flow is supersonic,

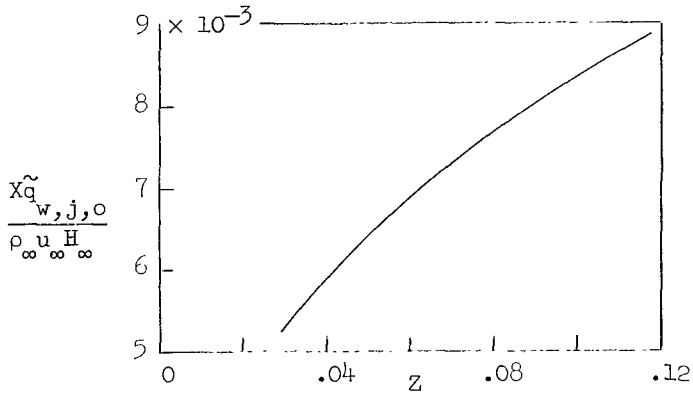

Figure 13.- Mean heat-transfer rate in jet mixing region. $M_\infty = 3.0$; $H_w/H_\infty = 0.3571$; $\dot{M} = 0$; $N_{Pr,t} = 1.0$.

the local heat-transfer rate is expected to decrease considerably as the local Mach number increases. This fact will be recognized more readily by considering the physical evidence that the maximum heating rate is encountered in the region of a sonic throat of a convergent-divergent supersonic nozzle.

In the case of an attached turbulent boundary layer, the local rate of energy transport increases considerably when compared with that of an attached laminar boundary layer, because the local mixing coefficient becomes of the order of ten times the laminar value for the same Reynolds numbers. Moreover, the growth of boundary-layer thickness has less effect on the local heating rate than the case with laminar flow, because $q_w \propto \delta^{-1/4}$ for turbulent flow whereas $q_w \propto \delta^{-1}$ for laminar flow. These unfavorable characteristics seem, therefore, to be largely responsible for the marked difference in heating rate between turbulent and laminar boundary-layer flows.

In the case of turbulent jet mixing which follows flow separation at a rearward-facing step, there seems to exist at least two favorable factors, where heat transfer is concerned. The one is that the external flow Mach number increases to a certain extent from its oncoming value through the Prandtl-Meyer expansion. Another is that the effective thickness of the viscous layer increases abruptly to the extent of the step height, although this effect may not be so efficient for turbulent boundary layers. In spite of these favorable factors, however, the turbulent jet mixing region has a marked unfavorable factor in that the local mixing coefficient increases considerably when compared with its value for attached boundary layer. This unfavorable factor seems to overcome the favorable factors and results in a net increase of heating rate in this region.

Figure 13 indicates that the mean heat-transfer rate in the jet mixing region increases with an increase in Z. This increase can be interpreted to mean that the heating rate increases with either an increase of oncoming boundary-layer thickness or a decrease of coolant slot height. The effect of coolant slot height can be understood rather easily. However, the effect of oncoming boundary-layer thickness given by the present approach may seem to be inconsistent with the general characteristics of the heat-transfer rate.

As has already been mentioned, strength of the Prandtl-Meyer expansion fan depends upon the value of Z if the oncoming flow Mach number is fixed and the coolant flow does not exist. Since the external flow Mach number M_1 decreases with an increase in Z, the rate of energy transport and the static temperature at the edge of the mixing layer also increase. The favorable factor of increasing thickness of the oncoming boundary layer is not very effective and the unfavorable factors predominate and result in a net increase of heating rate in the jet mixing region. Thus, the qualitative trend of the result shown in figure 13 is reasonable.

However, it is necessary to determine whether the quantitative magnitude of the mean heating rate is reasonable. Unfortunately, there exist neither theoretical results nor empirical data to compare with the present result. For this reason, the mean heat-transfer rate is approximated by use of a simple analogy, based on the result for an attached turbulent boundary layer. Detailed examination of turbulent boundary-layer characteristics on a flat plate reveals that the local heat-transfer rate is primarily proportional to the local mixing coefficient and the thickness of boundary layer in a form

$$\frac{q_w}{\rho_e u_e H_e} \propto \frac{K}{\delta^{1/4}}$$

Although the aerodynamic mechanism of separated flow may be essentially different from that of the attached flow, it is assumed for convenience that the heat-transfer rate associated with the separated flow can be expressed by this relation. Since the external-flow Mach number in the jet mixing region is different from its oncoming value, the effect of mass flow rate must be taken into consideration. Thus, the ratio of heat-transfer rate between the separated flow and the associated attached oncoming flow at the point of separation is given by the equation:

$$\frac{q_{w,s}}{q_{w,a}} = \frac{K_s}{K_a}\left(\frac{\delta_a}{\delta_s}\right)^{1/4} \frac{\rho_1 u_1}{\rho_\infty u_\infty}$$

where the subscripts s and a denote conditions appropriate to separated and attached flows, respectively, and the subscripts 1 and ∞ indicate conditions of external flow pertinent to jet mixing and oncoming regions. For simplicity, δ_a is assumed to be given by the thickness of the oncoming boundary layer δ_∞, and δ_s is assumed to be given by the sum of δ_∞ and the coolant slot height. Therefore,

$$\frac{\delta_a}{D} = \frac{\delta_\infty}{D} \approx 5Z$$

$$\delta_s = \delta_\infty + D$$

Under the conditions

$$M_\infty = 3.0$$

$$\frac{H_w}{H_\infty} = 0.3571$$

$$Z = 0.042$$

$$N_{Re,D} = 10^4$$

the oncoming boundary-layer thickness is estimated as

$$\frac{\delta_\infty}{D} = 0.21$$

The present approach gives as the value of mixing coefficient for separated flow

$$K_s = \frac{0.139}{X}$$

which seems to be nearly constant irrespective of the given conditions.

On the other hand, the mixing coefficient and the associated heat-transfer rate for attached oncoming flow are evaluated at $\delta_\infty/D = 0.21$ by use of flat-plate solutions given by Van Driest (ref. 17), which are obtained, respectively, as

$$K_a = 0.017$$

$$\frac{q_{w,a}}{\rho_\infty u_\infty H_\infty} = 1.49 \times 10^{-3}$$

Therefore, the estimated heat-transfer rate for the associated separated flow can be obtained for $X = 1$ as

$$\frac{q_{w,s}}{\rho_\infty u_\infty H_\infty} = 5.54 \times 10^{-3}$$

Similarly, the estimated heat-transfer rate can be obtained for other values of Z and the results are given in table I together with the present results of mean heating rate within the mixing region for comparison. As can be seen in the table, the order of magnitude of the present results is comparable with the estimated values, except that the present results are slightly larger than the estimated ones. However, in view of the fact that the estimated value corresponds to the local heating rate just downstream of

TABLE I.- COMPARISON OF THE PRESENT RESULTS WITH ESTIMATED HEAT-TRANSFER RATE

[$M = 3.0$, $H_w/H_\infty = 0.3571$, $K_s = 0.139/X$, $M = 0$, $N_{Pr,t} = 1.0$]

Z	$Xq_{w,s}/\rho_\infty u_\infty H_\infty$		$Xq_{w,s}/q_{w,a}$
	Present	Estimated	
0.042	5.99×10^3	5.54×10^3	3.72
.082	7.78	6.92	5.40
.101	8.38	7.32	6.00

separation point whereas the present result indicates a mean heating rate with the mixing region, small quantitative differences between these results are not important because the estimated value itself is only an approximate result. In any event, it seems that the present results will not differ much from the exact heat-transfer rate in the jet mixing region, if X is reasonable.

It is seen that the heating rate increases considerably in the separated region, when compared with that of the attached flow. This fact has already been pointed out by Chapman (ref. 20). According to his estimate, the heating rate for separated turbulent flow becomes nearly six times the attached flow value at $M_\infty = 0$ and this ratio decreases to 2.8 times that in the corresponding attached boundary layer at $M_\infty = 1.6$; thus the effect of Mach number is strong for turbulent flow. Chapman (ref. 21) further deduced that although this characteristic may be in sharp contradiction to the analogous comparison for the laminar case, the ratio will decrease considerably as the Mach number increases sufficiently. Since Chapman's evaluation is pertinent to the case of zero thickness of the oncoming boundary layer ($Z = 0$), a direct comparison between the present result and Chapman's data cannot be made. However, when it is considered that the ratio decreases with a decrease of Z, the present value of this ratio for $Z = 0.042$ seems to support Chapman's deduction.

However, it must be noted that there still remains a slight uncertainty in the quantitative value of the mean heat-transfer rate obtained in the present approach. Since the mean heating rate in the jet mixing region depends strongly upon the value of $\sigma_1\sqrt{N_{Re,L}}$ as is seen in equation (38), the choice of this value will modify the quantitative value of the mean heat-transfer rate. Although it has been evaluated by use of equation (15), there does not seem to exist in the present approach any rigorous proof that $X = 1.0$. In this sense, the present approach could be improved with better information on the flow properties of compressible turbulent jet mixing.

Figure 14 shows the effect of wall temperature on heating rate. As can be seen in figure 14, the mean heat-transfer rate without coolant flow decreases with an increase of wall enthalpy, and this trend is quite reasonable.

Figure 15 presents the variation of the mean heat-transfer rate in the jet mixing region with the coolant flow rate, and the effect of wall enthalpy is examined. Figure 15 clearly indicates that the coolant mass injection is effective in reducing the heating rate in this region, but the effectiveness itself seems to be small compared with the laminar case at the same blowing rate. This condition occurs because the energy input entrained from the external flow is much larger for turbulent mixing than for the laminar case. It can be seen that coolant mass injection becomes increasingly ineffective as the wall enthalpy decreases. This condition may result because the mixing layer becomes thin.

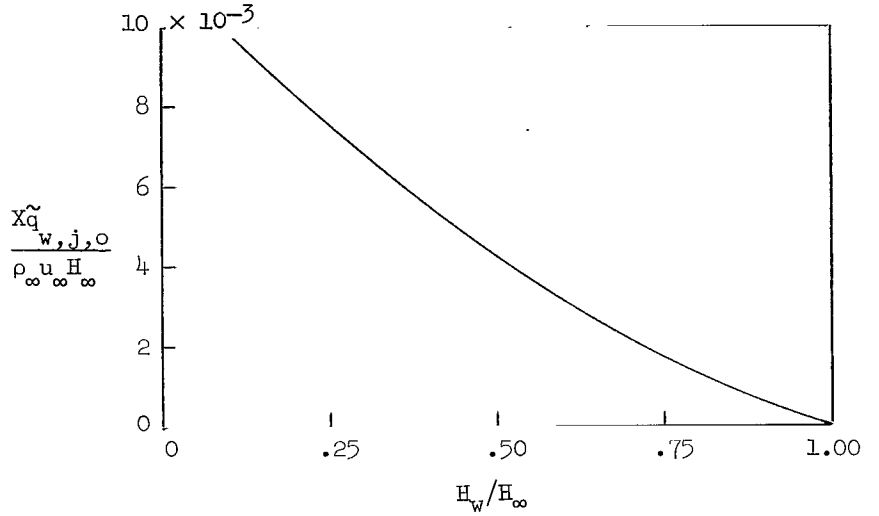

Figure 14.- Mean heat-transfer rate in jet mixing region. $M_\infty = 3.0$; $\dot{M} = 0$; $Z = 0.042$; $N_{Pr,t} = 1.0$.

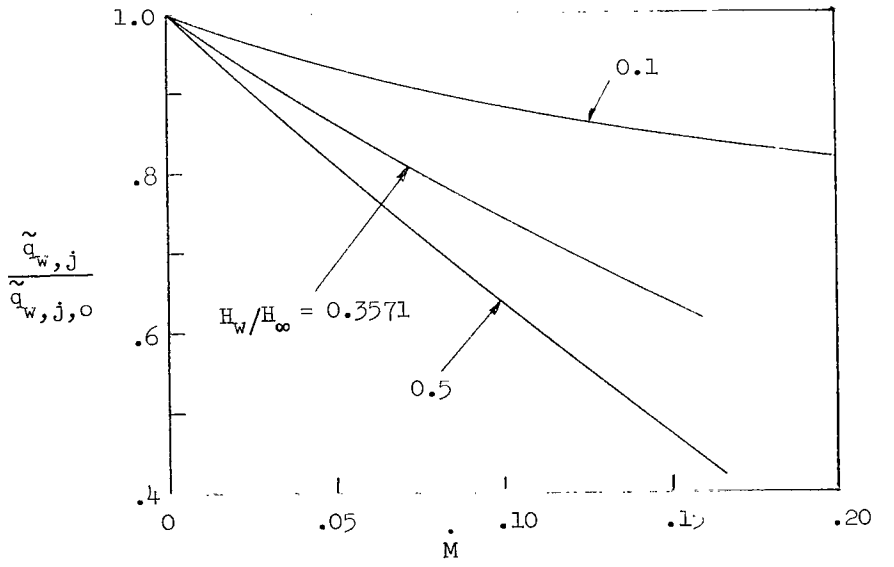

Figure 15.- Variation of mean heat-transfer rate in jet mixing region with coolant flow rate. $M_\infty = 3.0$; $H_c/H_w = 1.0$; $Z = 0.042$; $X = 1.0$; $N_{Pr,t} = 1.0$.

Figure 16 shows the effect of the parameter Z on the reduction of the mean heat-transfer rate. In figure 16, it can be seen that $\tilde{q}_{w,j}/\tilde{q}_{w,j,o}$ is rather insensitive to Z. Since the external flow Mach number varies less with coolant flow rate as Z grows, the rate of energy input from the external stream to the internal viscous layer becomes small for large values of Z. This characteristic seems to increase the effectiveness of coolant mass as a heat sink and, consequently, $\tilde{q}_{w,j}/\tilde{q}_{w,j,o}$ becomes insensitive to Z even if $\tilde{q}_{w,j,o}$ itself is large for a large value of Z.

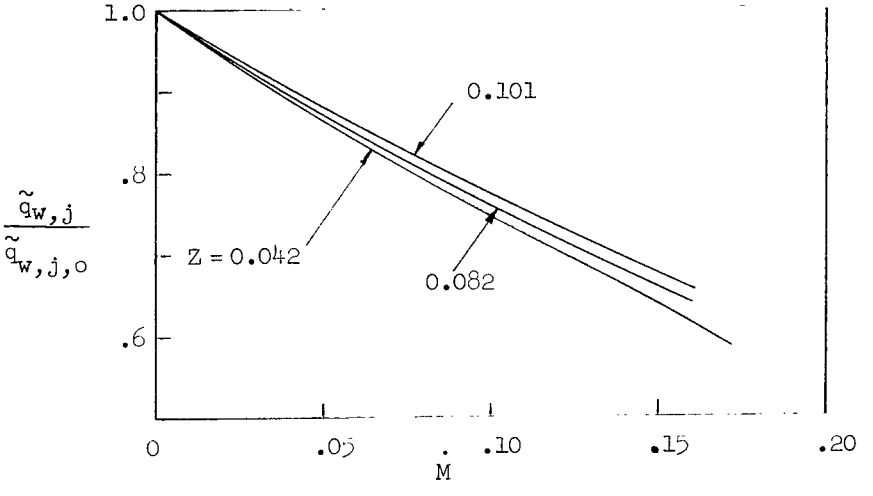

Figure 16.- Variation of mean heat-transfer rate in jet mixing region with coolant flow rate. $M_\infty = 3.0$; $H_w/H_\infty = 0.3571$; $H_c/H_w = 1.0$; $X = 1.0$; $N_{Pr,t} = 1.0$.

In order to demonstrate the effect of mixing coefficient on flow characteristics in the jet mixing region, the length of the separated region and the reduction of the mean heat-transfer rate with coolant flow rate were calculated for $X = 2$ and the results are shown, as examples, in figures 17 and 18, respectively; the results for $X = 1$ are also shown for comparison. As is seen in figure 17, the length of the separated region increases as the mixing coefficient decreases (large value of X). This condition is clearly due to the fact that the small mixing coefficient gives a small mixing-layer thickness and, consequently, elongates the separated region. However, as has been mentioned previously, the length of the separated region depends primarily upon the flow deflection angle which the external isentropic stream makes with the wall; as a result, the magnitude of the mixing coefficient has a relatively small influence on the length of the separated region.

On the other hand, the heat-transfer rate in this region is strongly influenced by the magnitude of the mixing coefficient. For instance, figure 13 shows that the mean heating rate for no coolant flow is inversely proportional to X and, hence, directly proportional

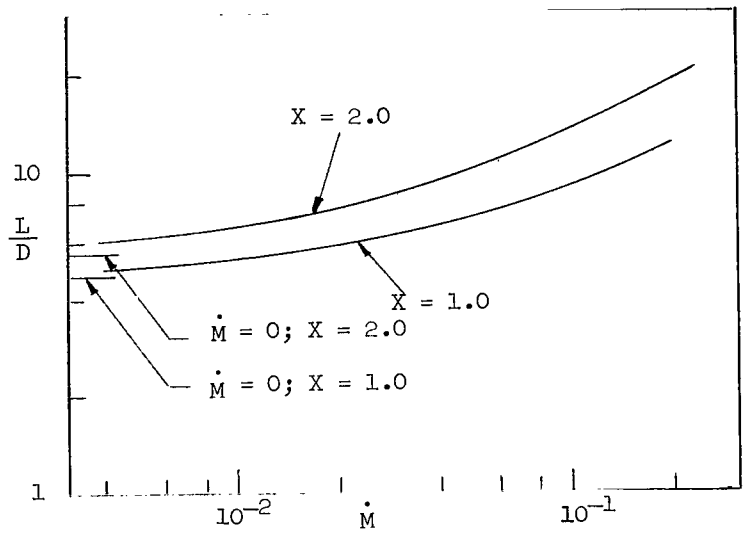

Figure 17.- Effect of mixing coefficient on length of separated region in jet mixing region. $M_\infty = 3.0$; $H_w/H_\infty = 0.3571$; $H_c/H_w = 1.0$; $Z = 0.042$; $N_{Pr,t} = 1.0$.

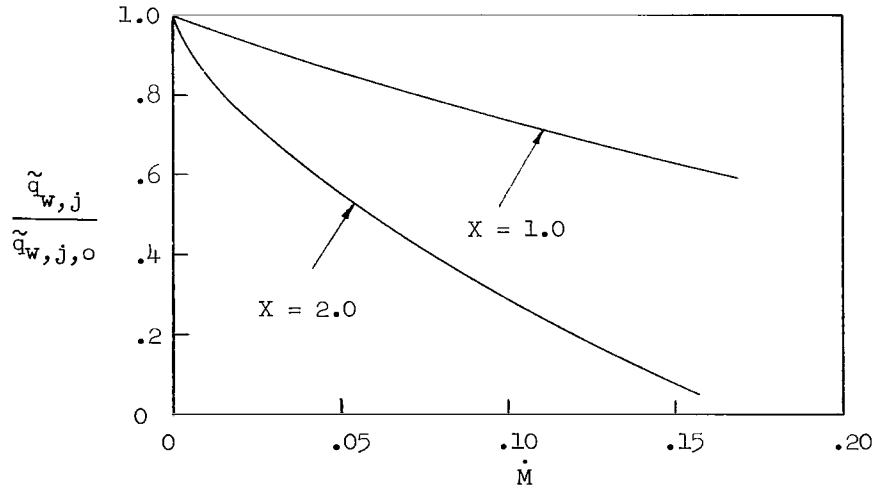

Figure 18.- Effect of mixing coefficient on mean heat-transfer rate in jet mixing region. $M_\infty = 3.0$; $H_w/H_\infty = 0.3571$; $H_c/H_w = 1.0$; $Z = 0.042$; $N_{Pr,t} = 1.0$.

to the mixing coefficient. In the case of coolant flow, the mixing coefficient strongly influences the reduction of the heating rate. (See fig. 18.) However, this result is quite natural because energy entrained in the mixing layer from the external stream decreases in proportion to the decrease of the mixing coefficient, whereas the effect of coolant mass as a heat sink remains the same for the same blowing rate and, consequently, $\tilde{q}_{w,j}/\tilde{q}_{w,j,o}$ decreases considerably with a small mixing coefficient.

From the viewpoint of practical application, small coolant slot height seems to be preferable. The results of the present approach suggest that to reduce the increase of heating rate in the jet mixing region compared with that in the corresponding attached boundary-layer flow, a smaller value of Z is obviously preferable. Therefore, if the height of the coolant slot is fixed for the intended blowing rate, the streamwise location of the slot should be near the leading edge, where the thickness of the oncoming boundary layer is small. The reasons for this location can be summarized as follows:

(1) The increase of mean heat-transfer rate for no coolant flow is decreased for smaller values of Z (fig. 13)

(2) The coolant flow efficiency increases (fig. 16)

(3) The length of the high heating region (length of separated region) decreases (fig. 11).

Recompression Region

The main difficulty which is encountered in numerical calculation for this region is evaluation of two parameters involved in the fundamental equations. These parameters are ϕ and K, which in principle should be functions of κ on the basis of the assumption of a one-parameter family for the boundary-layer state. Since there is neither analytical nor empirical information available for estimating these parameters at present, it is assumed that $\kappa = 0.03$ (Crocco and Lees' value) and $\phi = 1.0$ (flat-plate value).

Figure 19 shows a typical example of the variation of local pressure, heat-transfer rate, and boundary-layer thickness in the recompression region without coolant mass injection. For this case the origin of the x-axis is taken at the exit of this region and δ_p denotes the boundary-layer thickness at the exit. The subscript ∞ indicates conditions of the external flow in the region of the fully developed turbulent boundary layer downstream of recompression, which are assumed to be the same as the oncoming flow conditions. As can be seen in figure 19, the region of interaction spreads in a width more than eight times the boundary-layer thickness in this region. In the case of shock-wave—turbulent-boundary-layer interaction, it is generally recognized that the shock wave diffuses to a width of the order of 10 times the boundary-layer thickness, and this fact seems to support the present result.

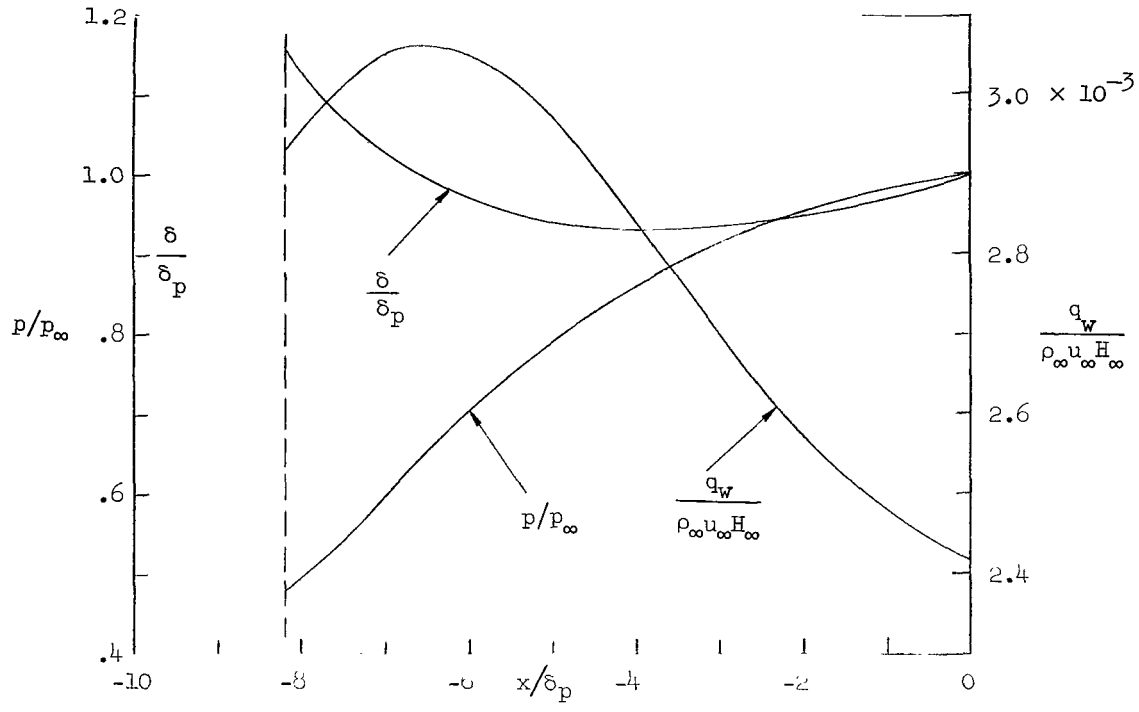

Figure 19.- Local pressure, thickness of boundary layer, and heating rate in recompression region. $M_\infty = 3.0$; $H_w/H_\infty = 0.3571$; $\dot{M} = 0$; $N_{Pr,t} = 1.0$.

Thickness of the boundary layer becomes a minimum at a distance downstream of the entrance of this region and most of the recompression takes place before the minimum thickness is approached. Moreover, it is interesting to see in the figure that the maximum heating rate occurs approximately at a point where the local pressure gradient becomes maximum. Furthermore, it should be remarked that this point does not coincide with the minimum boundary-layer thickness. These characteristics clearly indicate the physical fact that the local heat-transfer rate is more seriously influenced by pressure gradient (rate of change of external flow Mach number) than by local boundary-layer thickness. The decrease in local heating rate near the exit of the recompression region results from the combined effect of decrease in local pressure gradient and increase in boundary-layer thickness.

The boundary-layer thicknesses at the entrance and exit of the recompression region are points of interest. Figure 20 shows the effect of coolant flow rate on the boundary-layer thickness at both edges of the recompression region. As can be seen in figure 20, boundary-layer thickness at the exit is rather small compared with that at the entrance for a very small coolant flow rate. This result is quite reasonable because recompression is strong enough for a low coolant flow rate to contract the boundary-layer thickness, even if a certain amount of mass may be transported into the viscous layer from the external stream, as has been already shown in figure 19.

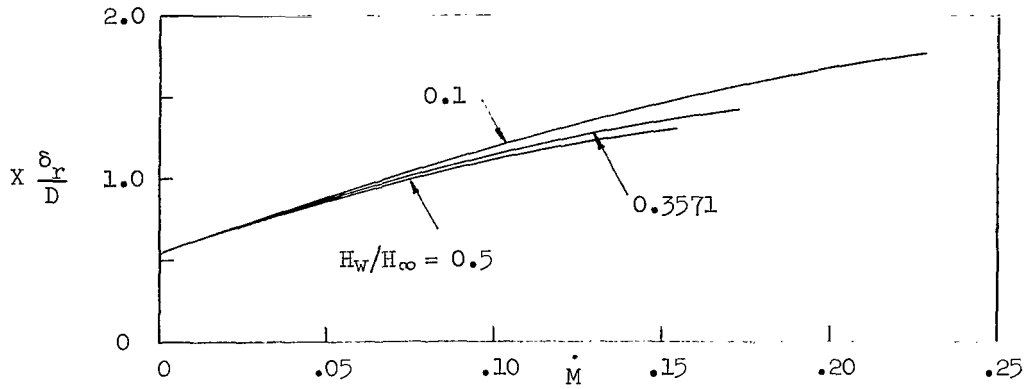

(a) Entrance of recompression region.

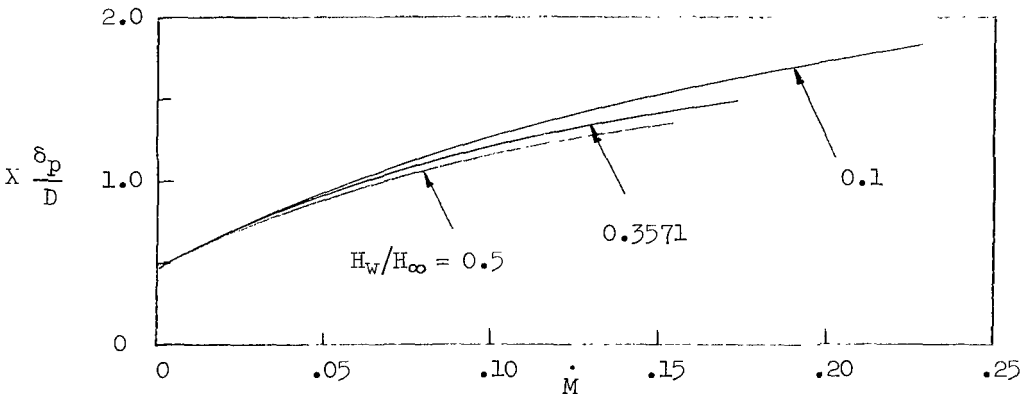

(b) Exit of recompression region.

Figure 20.- Thickness of boundary layer. $M_\infty = 3.0$; $H_c/H_w = 1.0$; $Z = 0.042$; $N_{Pr,t} = 1.0$.

The boundary-layer thickness at the entrance of the recompression region increases almost linearly with the blowing rate and is rather insensitive to wall enthalpy. Although a lower wall enthalpy decreases the thickness of the viscous layer, it also elongates the separated region, which, in turn, increases the mass input into the viscous layer and increases its thickness at the exit of the jet mixing region. These two effects seem to cancel one another, and thus result in the insensitivity to the wall enthalpy of the boundary-layer thickness at the entrance of the recompression region.

The difference between δ_p and δ_r shown in figure 20 indicates an increment of boundary-layer thickness through the recompression region, but it is fairly small in spite of the mass transport through mixing. This condition may be due to a contraction effect through recompression. Figure 21 presents the effect of Z on boundary-layer thickness at both edges of the recompression region. Since Z increases either with an increase of oncoming boundary-layer thickness or with a decrease of slot height, the results shown in this figure are reasonable.

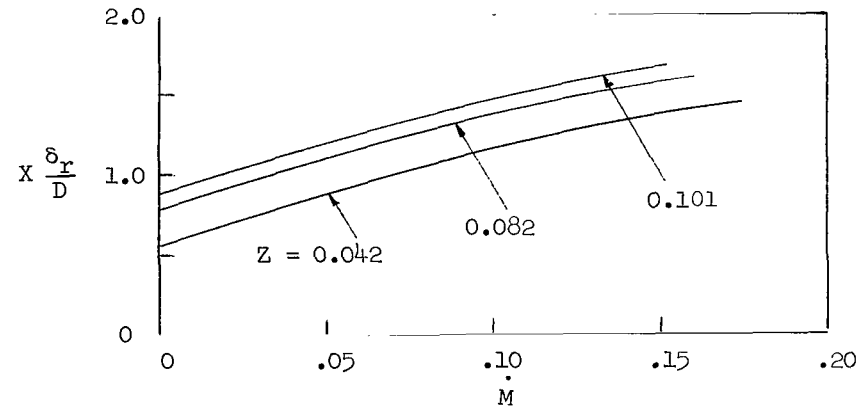

(a) Entrance of recompression region.

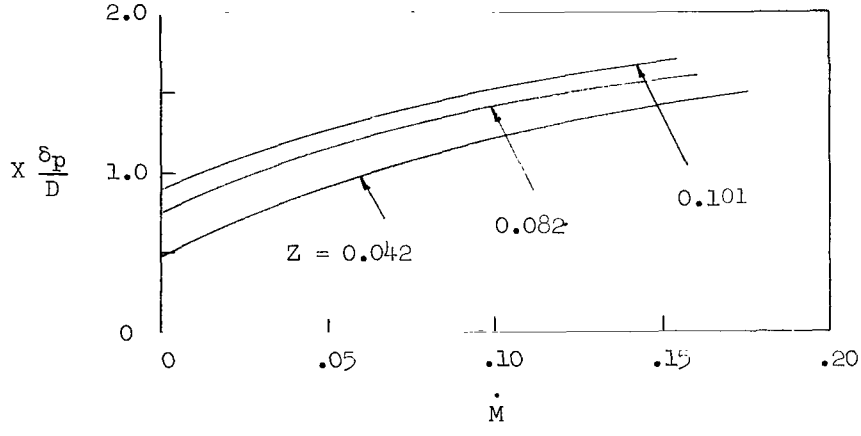

(b) Exit of recompression region.

Figure 21.- Thickness of boundary layer. $M_\infty = 3.0$; $H_w/H_\infty = 0.3571$; $H_c/H_w = 1.0$; $N_{Pr,t} = 1.0$.

The width of shock-wave diffusion (width of recompression region) is another point of interest. Figure 22 shows the variation of width in shock-wave diffusion with the coolant flow rate, where the effect of wall enthalpy and the parameter Z are examined separately. In the case of shock-wave—laminar-boundary-layer interaction, it is generally recognized that a lower wall enthalpy decreases the width of the shock-wave diffusion. The reason for this effect is that the extent of the subsonic region of the boundary layer near the wall, through which shock-wave disturbance may be felt upstream, decreases with decreasing wall temperature. The present results seem, at a glance, to be inconsistent with the general characteristic just mentioned, since, as seen in figure 22, the width of the shock-wave diffusion increases with a decrease of the wall enthalpy even in the case of no-coolant flow. However, detailed examination of the velocity profile across the jet mixing layer reveals that the low velocity region of the velocity profile tends to diffuse far inside the dead-air region as the wall enthalpy decreases, and thus indicates

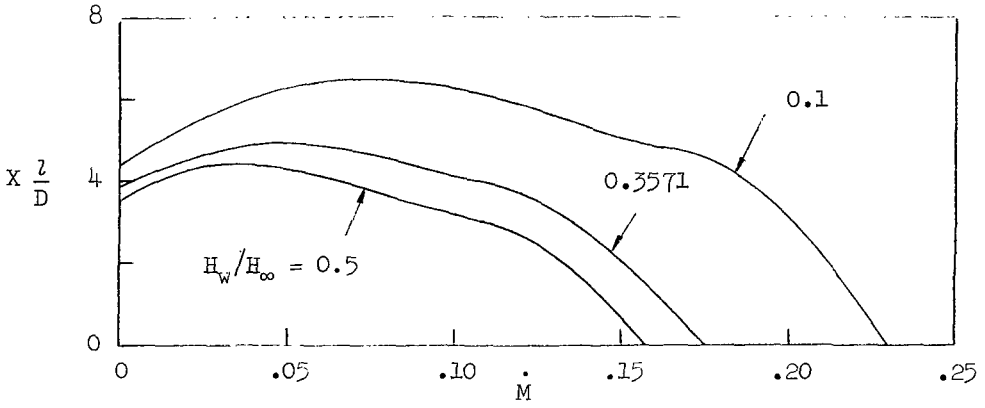

(a) $M_\infty = 3.0$; $H_c/H_w = 1.0$; $Z = 0.042$; $N_{Pr,t} = 1.0$.

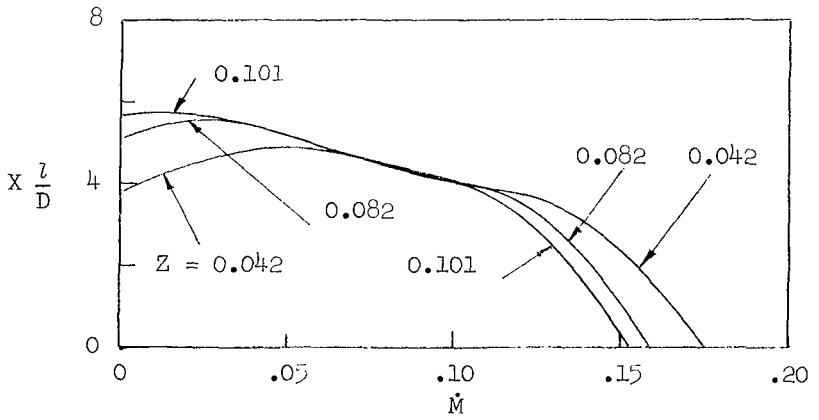

(b) $M_\infty = 3.0$; $H_w/H_\infty = 0.3571$; $H_c/H_w = 1.0$; $N_{Pr,t} = 1.0$.

Figure 22.- Width of shock wave diffusion.

an increase in the subsonic region. The same might be true for the attached turbulent boundary layer although there is no rigorous proof for this statement. Thus, this characteristic seems to overcome the decrease of the subsonic region due to decreased wall enthalpy and results in a net increase of the subsonic region through which the shock-wave disturbance may propagate upstream.

As the blowing rate increases, the effect of wall enthalpy on the width of the shock-wave diffusion seems, at a glance, to be pronounced. However, this condition is not due to the direct effect of wall enthalpy but mainly is due to differences in shock-wave strength for the same blowing rate. Since an increase in Z results in an increase of the boundary-layer thickness in the recompression region, the effect of Z on the width of the shock-wave diffusion is quite reasonable. (See fig. 22(b).)

Figures 23 and 24 where the effects of wall enthalpy and Z are examined separately present the mean heat-transfer rate without coolant mass injection in the recompression region. In contrast to the result shown in figure 13, the mean heat-transfer

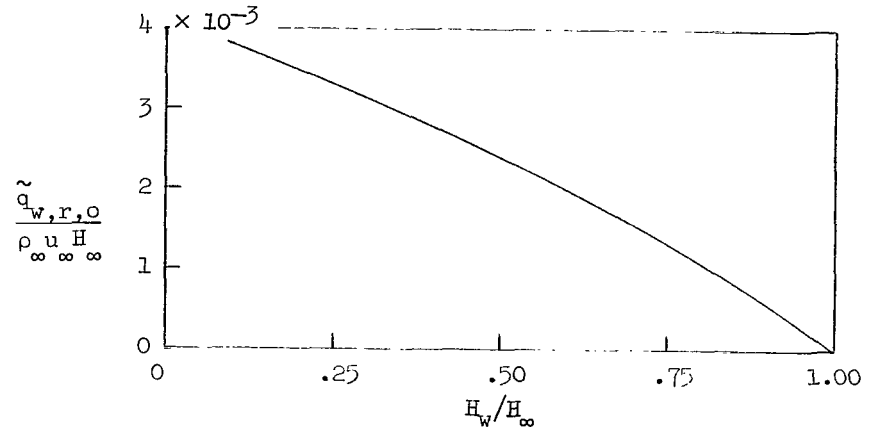

Figure 23.- Effect of enthalpy ratio on mean heat-transfer rate in recompression region. $M_\infty = 3.0$; $\dot{M} = 0$; $Z = 0.042$; $N_{Pr,t} = 1.0$.

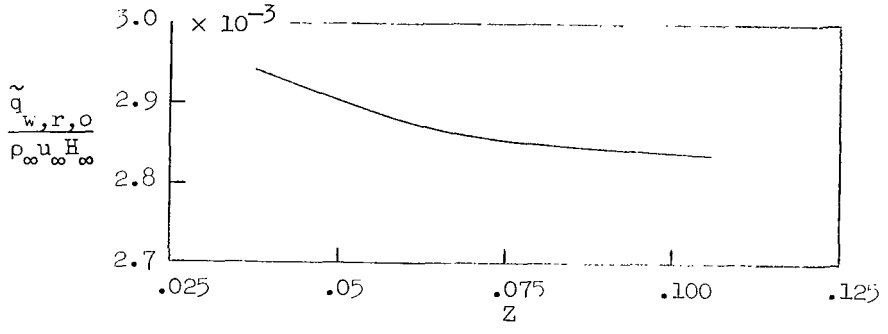

Figure 24.- Mean heat-transfer rate in recompression region. $M_\infty = 3.0$; $\dot{M} = 0$; $H_w/H_\infty = 0.3571$; $N_{Pr,t} = 1.0$.

rate in the recompression region decreases slightly with increased Z, as can be seen in figure 24. Clearly, the shock-wave strength decreases with increased Z, whereas the width of the shock-wave diffusion increases. This characteristic obviously indicates that the local pressure gradient decreases considerably with an increase in Z and, consequently, the maximum value of the local heating rate within the recompression region decreases to yield a net decrease of mean heating rate.

Figure 25 in which the effect of wall enthalpy is examined shows the variation of the mean heat-transfer rate with the coolant flow rate. The mean heating rate decreases with an increase in coolant flow rate. However, since the mixing between the coolant flow and the oncoming flow has almost finished before the recompression region is approached, it seems that the coolant mass no longer acts as a heat sink in this region, but only contributes to increased boundary-layer thickness; therefore, the effectiveness of coolant flow, expressed as $\tilde{q}_{w,R}/\tilde{q}_{w,R,o}$ becomes higher compared with its value in the jet

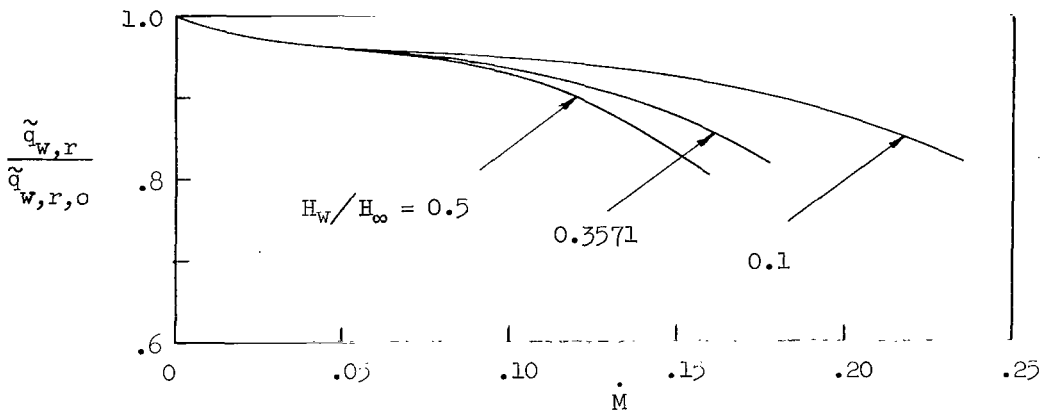

Figure 25.- Variation of mean heat-transfer rate in recompression region with coolant flow rate for various enthalpy ratios. $M_\infty = 3.0$; $H_c/H_w = 1.0$; $Z = 0.042$; $N_{Pr,t} = 1.0$.

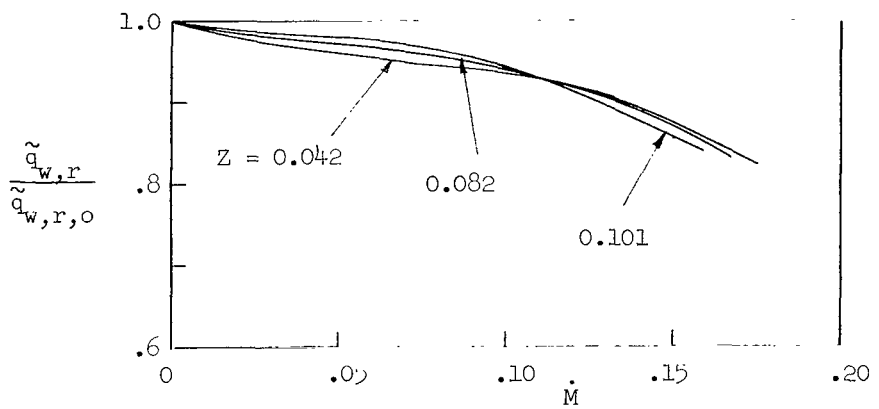

Figure 26.- Variation of mean heat-transfer rate in recompression region with coolant flow rate. $M_\infty = 3.0$; $H_w/H_\infty = 0.3571$; $H_c/H_w = 1.0$; $N_{Pr,t} = 1.0$.

mixing region. Figure 26 shows the effect of Z on heating rate in the recompression region and indicates that the mean heat-transfer-rate ratio seems to be insensitive to Z in this region as well as in the jet mixing region.

As has been mentioned previously, the local heat-transfer rate depends strongly upon the local rate of energy transport into the internal viscous layer from the external isentropic stream. This dependence can be interpreted to mean that the local heating rate is seriously influenced by the order of magnitude of the local mixing coefficient. In order to demonstrate this effect, the mean heat-transfer rate in the recompression region is plotted against the mixing coefficient in figure 27, where the shock-wave strength and wall enthalpy are fixed and no coolant mass injection is assumed. Figure 27 shows that the mean heat-transfer rate decreases considerably as the mixing coefficient decreases.

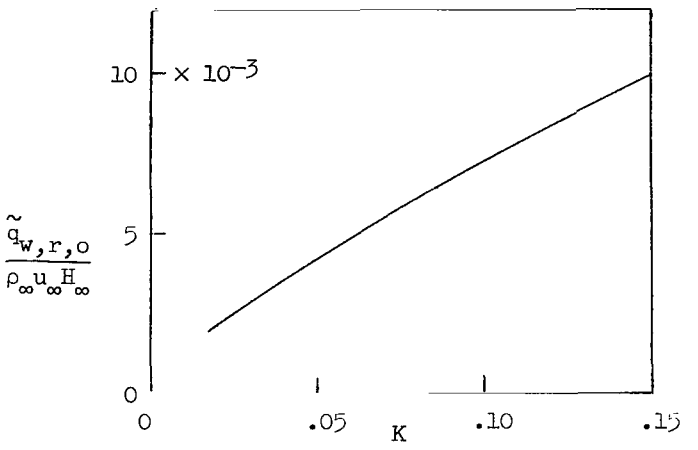

Figure 27.- Effect of mixing coefficient on mean heat-transfer rate in recompression region. $M_\infty = 3.0$; $H_w/H_\infty = 0.3571$; $M_1 = 3.514$; $\dot{M} = 0$; $Z = 0.042$; $N_{Pr,t} = 1.0$.

In the preceding section, a qualitative discussion on heating rate of turbulent boundary layer has shown that

$$\tilde{q}_w \propto K\delta^{-1/4}$$

The thickness of the boundary layer is proportional to the mass flux across the boundary layer, and the mass flux, in turn, is proportional to the mixing coefficient. Therefore, the relation may be reexpressed as

$$\tilde{q}_w \propto K^{3/4}$$

Hence,

$$\frac{\tilde{q}_{w,2}}{\tilde{q}_{w,1}} = \left(\frac{K_2}{K_1}\right)^{3/4} \tag{107}$$

where $\tilde{q}_{w,1}$ and $\tilde{q}_{w,2}$ denote the mean heating rates corresponding to K_1 and K_2, respectively. Examination of the result shown in figure 27 clearly reveals that equation (107) is a fair approximation. This result supports the validity of the discussion made in the preceding section on the characteristic behavior of the mean heat-transfer rate in the jet mixing region.

Figure 28, where the effects of wall enthalpy and the parameter Z are examined, shows the variation of coolant flow Mach number at the slot exit at which the recompression shock waves disappear. The critical coolant flow Mach number M_c^*, defined by the disappearance of the recompression shock wave, increases with either an increase in wall enthalpy or a decrease in Z. Reference 4 found experimentally that for isoenergetic

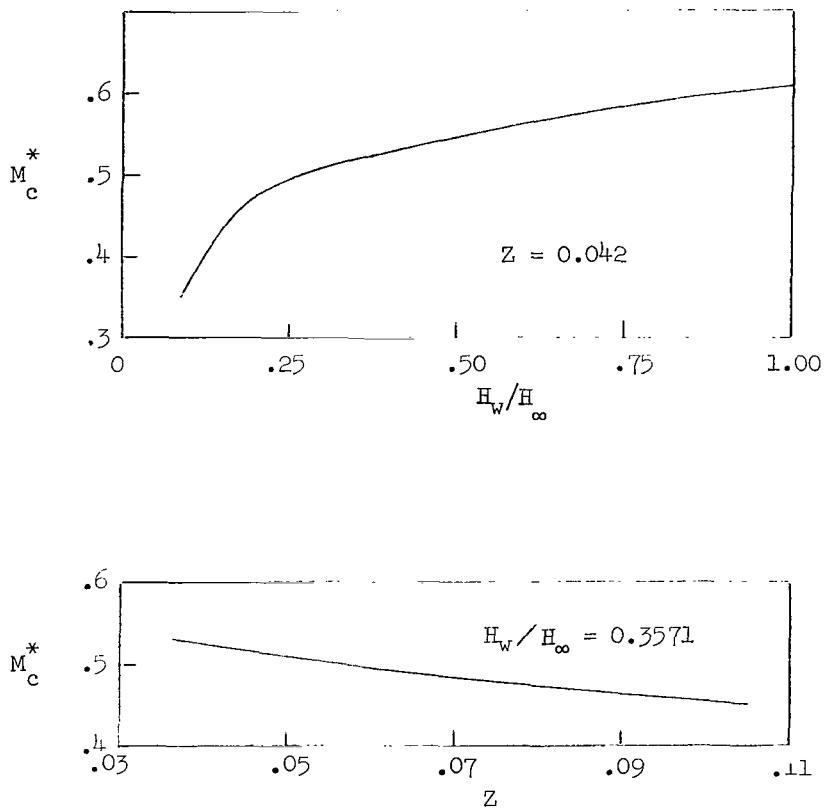

Figure 28.- Coolant flow Mach number at slot exit for disappearance of shock wave. $M_\infty = 3.0$; $H_c/H_w = 1.0$; $X = 1.0$; $N_{Pr,t} = 1.0$.

injection $(H_c = H_\infty)$ and $Z = 0.02$, the disappearance of the recompression shock wave occurs before the choking condition of coolant flow is approached at the slot exit. This condition means that the critical Mach number remains subsonic. A rough evaluation shows that the critical coolant flow Mach number is about 0.65. This value is supported at least qualitatively by the experiment.

Region of Fully Developed Turbulent Boundary Layer and Overall Results

Reduced heat transfer in the region of a fully developed turbulent boundary layer results from the growth of boundary-layer thickness associated with the coolant mass injection upstream. Since the Mach number of the external stream is assumed to be kept constant at its oncoming value, a complicated flow phenomenon due to change in the external flow Mach number does not appear in this region. Moreover, a large amount of mass transport from the external stream to the internal dissipative flow in the upstream regions, which has been shown to have rather unfavorable effects on heating rate in the upstream regions, becomes a favorable factor in this region and results in reduction of local heat-transfer rate. This net reduction of overall heat transfer seems to be a characteristic of film cooling through a rearward-facing slot.

Figures 29 and 30, where the effects of wall enthalpy and slot height are examined, respectively, show local effectiveness of film cooling in the region of the fully developed turbulent boundary layer. The local effectiveness of film cooling in this region decreases monotonically with increasing coolant flow rate. The reason may be understood through the subsequent argument.

Since the local heat-transfer rate is approximately proportional to $\delta^{-1/4}$, it is easily shown that

$$\frac{q_w}{q_{w,o}} \propto \left(\frac{\delta_o}{\delta}\right)^{1/4} \tag{108}$$

where the subscript o denotes conditions of no coolant flow. As can be seen in figures 20 and 21, the boundary-layer thickness δ_p at the entrance of this region increases with increase of coolant flow, but the rate of increase becomes smaller as the blowing rate grows. These characteristics clearly indicate that the rate of increase of the

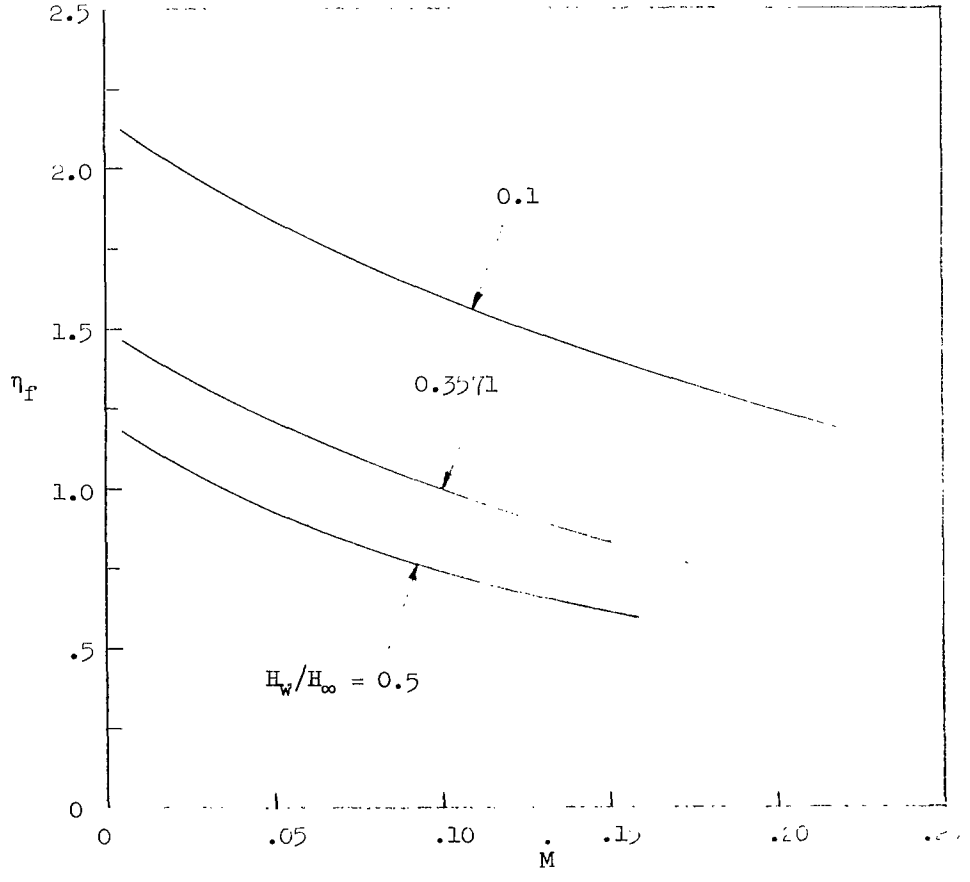

Figure 29.- Local effectiveness of film cooling in region of fully developed turbulent boundary layer. $M_\infty = 3.0$; $H_c/H_w = 1.0$; $Z = 0.042$; $N_{Re,D} = 10^4$; $X = 1.0$; $N_{Pr,t} = 1.0$.

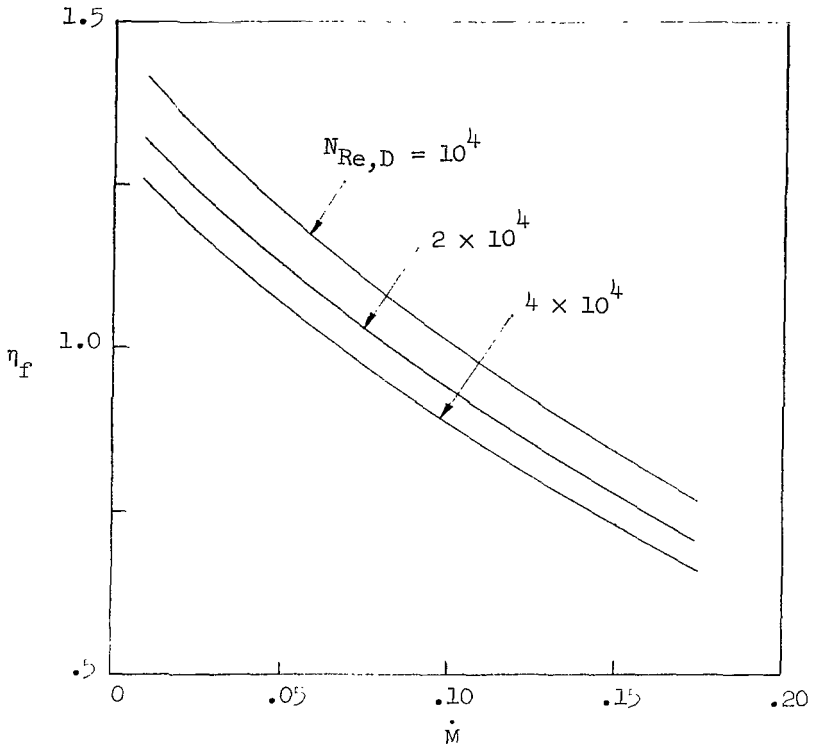

Figure 30.- Local effectiveness of film cooling in region of fully developed turbulent boundary layer. $M_\infty = 3.0$; $H_w/H_\infty = 0.3571$; $H_c/H_w = 1.0$; $Z = 0.042$; $X = 1.0$; $N_{Pr,t} = 1.0$.

numerator in equation (100) is less than $\dot{M}$ except in the vicinity of zero coolant flow rate, where it is of the order of $\dot{M}$, whereas the denominator is always of the order of $\dot{M}$. Therefore, η_f is finite at $\dot{M} = 0$ and decreases monotonically as $\dot{M}$ grows.

The effect of wall enthalpy on η_f shown in figure 29 seems to be physically reasonable because the heat-transfer reduction is proportional to $H_\infty - H_w$. It is interesting to see in figure 30 that a smaller coolant slot height may be more effective. However, attention must be paid to the fact that the results shown in figure 30 do not indicate a pure effect of slot height, since the change of $N_{Re,D}$, the value of Z being kept unchanged, means a change in thickness of the oncoming boundary layer at the same time. It is clear that a decrease of $N_{Re,D}$, Z being kept unchanged, means a decrease of δ_∞, and indicates an upstream movement of the coolant slot location. This condition means a thin boundary layer at the entrance of the region of the fully developed turbulent boundary layer. In any event, the local heating rate decreases rather slowly, as is seen in the relation (108), with an increase of boundary-layer thickness due to coolant flow rate.

It must be noted that in the region of the fully developed turbulent boundary layer, the magnitude of the local heat-transfer-rate reduction due to an increase of

boundary-layer thickness is not so large because $q_w \propto \delta^{-1/4}$. However, since the region of integration used for obtaining η_f extends to infinity, the local effectiveness of film cooling in this region seems to become rather large. In fact, if an observation point for the local effectiveness of film cooling is taken at a finite distance downstream of the entrance of this region, then η_f will decrease considerably depending upon the location of the observation point.

Figures 31(a) to 31(c) present the overall effectiveness of film cooling for wall enthalpy ratios of 0.5, 0.3571, and 0.1, respectively. The overall effectiveness of film cooling η_T has an explicit physical meaning of total heat-transfer reduction pertinent to whole flow field downstream of the injection point. Therefore, it can be considered as a useful quantitative measure to indicate efficiency of the injected coolant mass.

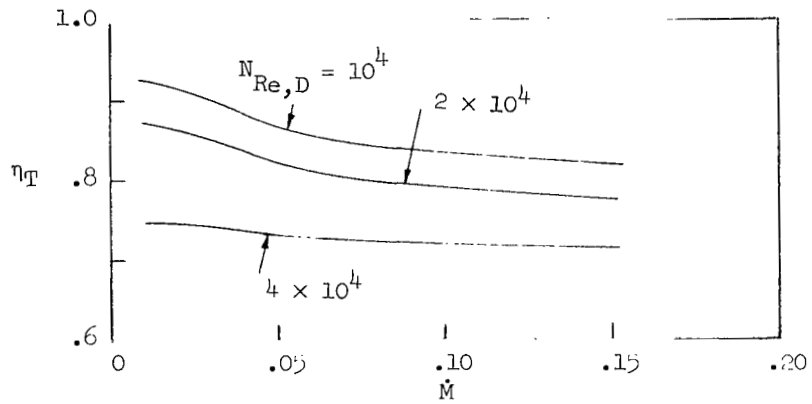

(a) $M_\infty = 3.0$; $H_w/H_\infty = 0.5$; $H_c/H_w = 1.0$; $Z = 0.042$; $X = 1.0$; $N_{Pr,t} = 1.0$.

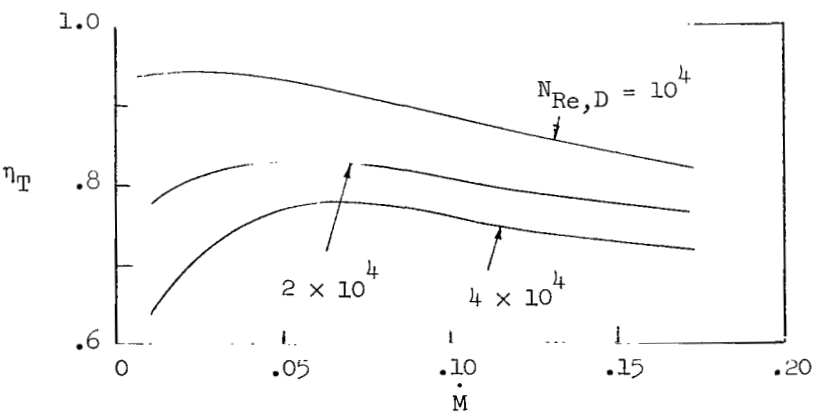

(b) $M_\infty = 3.0$; $H_w/H_\infty = 0.3571$; $H_c/H_w = 1.0$; $Z = 0.042$; $X = 1.0$; $N_{Pr,t} = 1.0$.

Figure 31.- Overall effectiveness of film cooling.

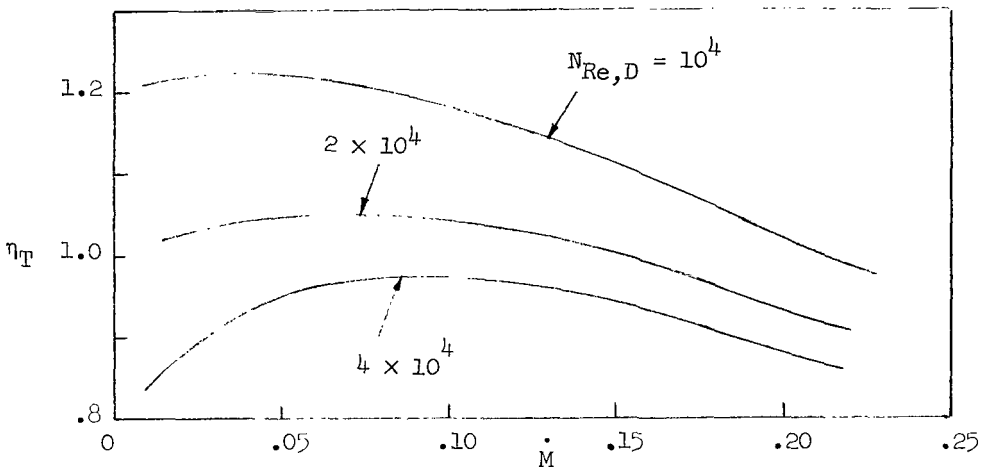

(c) $M_\infty = 3.0$; $H_w/H_\infty = 0.1$; $H_c/H_w = 1.0$; $Z = 0.042$; $X = 1.0$; $N_{Pr,t} = 1.0$.

Figure 31.- Concluded.

It is interesting to see in figure 31 that the magnitude of the overall effectiveness of film cooling becomes small compared with η_f for low coolant flow rates, whereas it becomes larger than η_f as the blowing rate grows. This result clearly indicates the effect of the jet mixing and recompression regions. The mean heating rate in these high heating regions decreases monotonically with an increase in the coolant flow rate, but their length increases with blowing rate, for small blowing rates. These characteristics increase the net heat transfer to the wall within the high heating regions in the case of small coolant flow rate, and thus decrease η_T. On the other hand, as the blowing rate goes beyond a certain value, the mean heat-transfer rate within the high heating regions is still decreasing, whereas the total length of these regions becomes insensitive to coolant flow rate, so that the overall heating decreases. As a result, η_T reaches its maximum at a certain blowing rate which is dependent on wall enthalpy and $N_{Re,D}$.

In order to confirm this point, the effect of wall enthalpy on η_T is examined by keeping other conditions constant and the result is shown in figure 32. The lower wall enthalpy seems to increase slightly the coolant flow rate at which η_T reaches a maximum. Figure 33 presents an examination of the effect of the oncoming boundary-layer thickness on η_T. Since $N_{Re,D}$ is kept constant, the increase of Z indicates an increase of δ_∞. As is seen in figure 33, a small thickness of the oncoming boundary layer is favorable for increasing the overall effectiveness of film cooling, but the coolant flow rate for a maximum η_T is less sensitive to the oncoming boundary-layer thickness.

Figure 34 shows the effect of the coolant slot height on the overall effectiveness of film cooling. The figure clearly indicates that a larger slot height results in a larger coolant flow rate at which η_T becomes a maximum. Therefore, it may be concluded

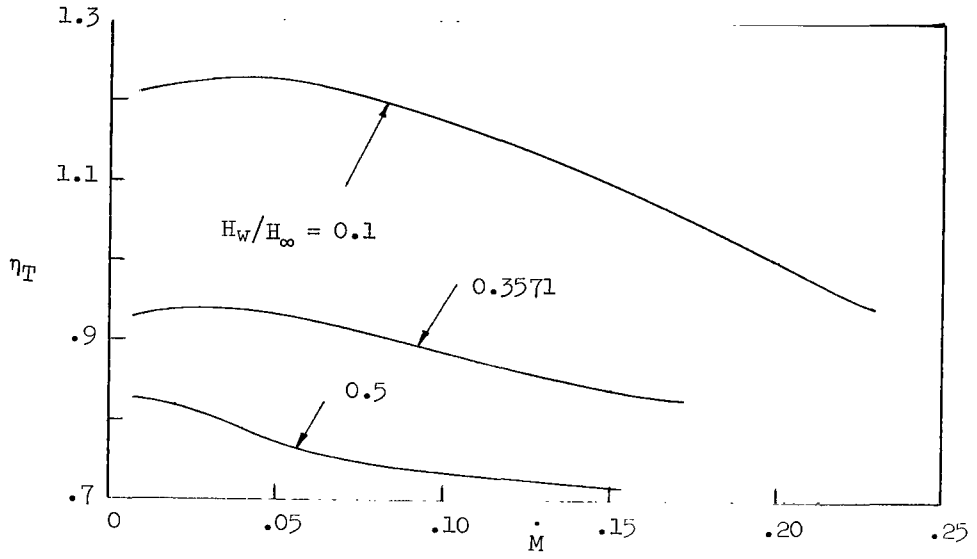

Figure 32.- Overall effectiveness of film cooling for various enthalpy ratios. M_∞ = 3.0; H_c/H_w = 1.0; Z = 0.042; $N_{Re,D} = 10^4$; X = 1.0; $N_{Pr,t}$ = 1.0.

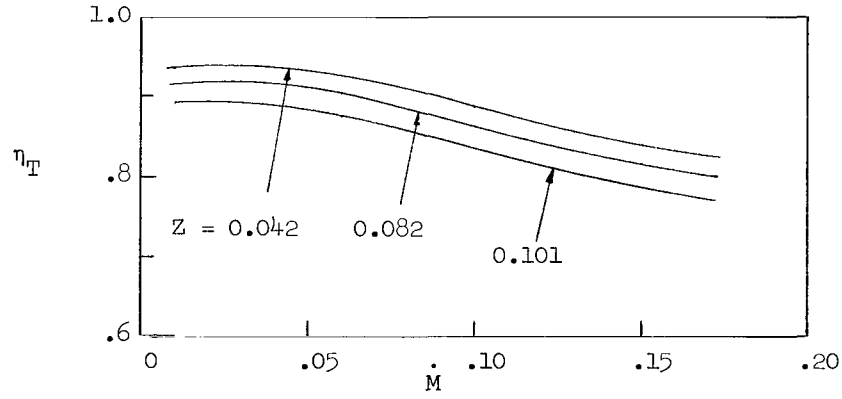

Figure 33.- Overall effectiveness of film cooling for various values of Z. M_∞ = 3.0; H_w/H_∞ = 0.3571; H_c/H_w = 1.0; $N_{Re,D} = 10^4$; X = 1.0; $N_{Pr,t}$ = 1.0.

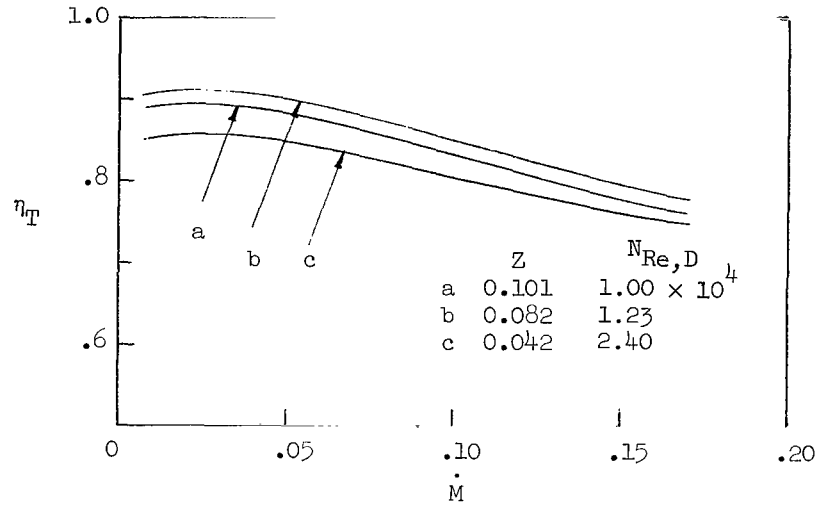

Figure 34.- Overall effectiveness of film cooling for selected conditions. $M_\infty = 3.0$; $H_w/H_\infty = 0.3571$; $H_c/H_w = 1.0$; $X = 1.0$; $N_{Pr,t} = 1.0$.

that the blowing rate for maximum overall effectiveness of film cooling increases with increased slot height, and this trend becomes increasingly pronounced as the wall enthalpy decreases.

It should be noted that there exists an optimum value of the coolant slot height for which the overall effectiveness becomes a maximum if the other conditions are fixed. In the regions of jet mixing and recompression, the coolant slot height determines the flow characteristics, mainly in a form of $Z \left(= \frac{C}{D\sqrt[n]{N_{Re}}}\right)$, whereas in the region of fully developed turbulent boundary layer, it determines the flow characteristics in forms of Z and D itself. Since a complicated nonlinear coupling of these factors is an essential physical feature of the overall effectiveness of film cooling, it is not easy to give a comprehensive argument on the physical reason for the existence of an optimum coolant slot height. For this reason, a simple discussion is given to assist in understanding the present result.

Insofar as the present problem is concerned, the overall effectiveness of film cooling can be considered to be a function of Z, D, and $\dot{M}$:

$$\eta_T = f_n(Z,D,\dot{M})$$

Differentiation of η_T with respect to D leads to

$$\frac{d\eta_T}{dD} = \left(\frac{\partial f_n}{\partial D}\right)_Z + \left(\frac{\partial f_n}{\partial Z}\right)_D \frac{dZ}{dD} \tag{109}$$

It is obvious from figure 31(b) that the first derivative on the right-hand side of equation (109) is always negative. In the same way, the second derivative is always negative from the results shown in figure 33, whereas the third derivative is also negative. These characteristics suggest implicitly that $d\eta_T/dD$ might vanish at a certain finite value of D, and thus indicate that η_T has an extremum, which will be found to be a maximum from a rough examination.

CONCLUDING REMARKS

Heat transfer downstream of a two-dimensional rearward-facing step with coolant injection has been analyzed under the assumption that the oncoming boundary-layer thickness is small compared with the step height, and the coolant flow rate is so small that the velocity in the dead-air region is negligible. The whole flow field is divided into three regions: a jet mixing region, a recompression region, and a fully developed turbulent boundary layer far downstream.

The flow field in the jet mixing region is shown to be determined uniquely for given conditions, and the pressure in this region increases with increased coolant flow. The length of the separated region also increases with increased blowing rate, is fairly sensitive to the oncoming flow conditions, and is rather insensitive to wall enthalpy. With no coolant flow, the mean heat-transfer rate within this region increases considerably compared with that in the corresponding attached boundary-layer flow. However, the mean heating rate decreases with the increased coolant flow.

The increase in local heating rate compared with that in the corresponding flat-plate flow is shown to be inevitable in the recompression region, because of a strong adverse pressure gradient, and the local heating rate reaches a maximum at the point within this region where the local pressure gradient also is highest. The mean heat-transfer rate within this region decreases with increased blowing rate. However, in contrast to the jet mixing region, the decrease in mean heat-transfer rate is not large in this region. Thus, the jet mixing and recompression regions have a rather high heating rate compared with the corresponding flat-plate flow.

The increased heating in these upstream regions is shown to be compensated sufficiently in the region of a fully developed turbulent boundary layer; as a result, the film cooling is fairly effective in reducing the overall heat transfer to the wall. It is shown that a smaller thickness of the oncoming boundary layer gives higher effectiveness of film cooling, and indicates that the upstream location of coolant slot is preferable.

The overall effectiveness of film cooling, which increases with increased slot height, reaches a maximum at a very small coolant flow rate; this optimum blowing rate

depends slightly upon the wall enthalpy. The present approach further indicates that if the thickness of the oncoming boundary layer is fixed, there exists an optimum height of the coolant slot for which the overall cooling effectiveness is a maximum.

Langley Research Center,
National Aeronautics and Space Administration,
Hampton, Va., July 29, 1970.

APPENDIX

SOLUTION OF FUNDAMENTAL EQUATIONS IN JET MIXING REGION

If $u^*/h^{*2} = f(\zeta)$ is assumed to be known, equation (9) can be written in a form

$$f\frac{d^2u^*}{d\zeta^2} + (\zeta + f')\frac{du^*}{d\zeta} = 0 \tag{A1}$$

where the prime indicates differentiation with respect to ζ. Equation (A1) is an ordinary differential equation of the second order; thus, a general solution can be easily obtained as

$$u^* = C_1 \int_0^\zeta \frac{F}{f}\, d\zeta + C_2 \tag{A2}$$

where

$$F(\zeta) = \exp\left(-\int_0^\zeta \frac{\zeta}{f}\, d\zeta\right) \tag{A3}$$

and where C_1 and C_2 are integration constants to be determined by the given boundary conditions. From equations (12)

$$\left.\begin{aligned} 1 &= C_1 \int_0^\infty \frac{F}{f}\, d\zeta + C_2 \\ 0 &= C_1 \int_0^{-\infty} \frac{F}{f}\, d\zeta + C_2 \end{aligned}\right\} \tag{A4}$$

which yields

$$\left.\begin{aligned} C_1 &= \frac{1}{\int_{-\infty}^{\infty} \frac{F}{f}\, d\zeta} = \hat{\beta} \\ C_2 &= 1 - \hat{\beta} \int_0^\infty \frac{F}{f}\, d\zeta \end{aligned}\right\} \tag{A5}$$

Therefore, the solution for $u^*(\zeta)$ satisfying the given boundary conditions can be obtained as

$$u^*(\zeta) = \hat{\beta} \int_{-\infty}^{\zeta} \frac{F}{f}\, d\zeta \tag{A6}$$

APPENDIX

The solution for $h^*(\zeta)$ can be obtained similarly. Rewriting equation (10) yields the following ordinary differential equation of the second order, since $u^*(\zeta)$ has been known from equation (A6),

$$f\frac{d^2h^*}{d\zeta^2} + \left(N_{Pr,t}\zeta + f'\right)\frac{dh^*}{d\zeta} = -N_{Pr,t}(\gamma - 1)M_1{}^2 f\left(\frac{du^*}{d\zeta}\right)^2 \tag{A7}$$

Since

$$\frac{du^*}{d\zeta} = \hat{\beta}\frac{F}{f}$$

a general solution to equation (A7) may be obtained as

$$h^* = C_3\int_{-\infty}^{\zeta}\frac{F^{N_{Pr,t}}}{f}\,d\zeta - \hat{\beta}^2 N_{Pr,t}(\gamma - 1)M_1{}^2\int_{-\infty}^{\zeta}\frac{F^{N_{Pr,t}}}{f}\int_0^{\xi}\frac{F^{2-N_{Pr,t}}}{f}\,d\eta\,d\xi + C_4 \tag{A8}$$

where C_3 and C_4 are integration constants. From equations (12)

$$\left.\begin{aligned} 1 &= C_3\int_{-\infty}^{\infty}\frac{F^{N_{Pr,t}}}{f}\,d\zeta - \hat{\beta}^2 N_{Pr,t}(\gamma - 1)M_1{}^2\int_{-\infty}^{\infty}\frac{F^{N_{Pr,t}}}{f}\int_0^{\xi}\frac{F^{2-N_{Pr,t}}}{f}\,d\eta\,d\xi + C_4 \\ h_c{}^* &= C_4 \end{aligned}\right\} \tag{A9}$$

which leads to

$$C_3 = \frac{1}{\displaystyle\int_{-\infty}^{\infty}\frac{F^{N_{Pr,t}}}{f}\,d\zeta}\left[1 - h_c{}^* + \hat{\beta}^2 N_{Pr,t}(\gamma - 1)M_1{}^2\int_{-\infty}^{\infty}\frac{F^{N_{Pr,t}}}{f}\int_0^{\xi}\frac{F^{2-N_{Pr,t}}}{f}\,d\eta\,d\xi\right] \tag{A10}$$

Thus, the solution for $h^*(\zeta)$ satisfying the given boundary conditions can be expressed as

$$h^*(\zeta) = h_c{}^* - \hat{\beta}^2 N_{Pr,t}(\gamma - 1)M_1{}^2\int_{-\infty}^{\zeta}\frac{F^{N_{Pr,t}}}{f}\int_0^{\xi}\frac{F^{2-N_{Pr,t}}}{f}\,d\eta\,d\xi + C_3\int_{-\infty}^{\zeta}\frac{F^{N_{Pr,t}}}{f}\,d\zeta \tag{A11}$$

where C_3 has been given by equation (A10).

REFERENCES

1. Milford, C. M.; and Spiers, D. M.: An Investigation Into Film Cooling by Slots. International Developments in Heat Transfer. Amer. Soc. Mech. Eng., c.1963, pp. 669-674.

2. Carter, Howard S.: Water-Film Cooling of an 80° Total-Angle Cone at a Mach Number of 2 for Airstream Total Temperatures Up to 3000° R. NASA TN D-2029, 1963. (Supersedes NASA MEMO 12-27-58L.)

3. Eckert, E. R. G.; and Birkebak, R. C.: The Effects of Slot Geometry on Film Cooling. Heat-Transfer, Thermodynamics, and Education, H. A. Johnson, ed., McGraw-Hill Book Co., Inc., c.1964, pp. 150-163.

4. Goldstein, R. J.; Eckert, E. R. G.; Tsou, F. K.; and Haji-Sheikh, A.: Film Cooling With Air and Helium Injection Through a Rearward-Facing Slot Into a Supersonic Air Flow. AIAA J., vol. 4, no. 6, June 1966, pp. 981-985.

5. Hatch, James E.; and Papell, S. Stephen: Use of a Theoretical Flow Model To Correlate Data for Film Cooling or Heating an Adiabatic Wall by Tangential Injection of Gases of Different Fluid Properties. NASA TN D-130, 1959.

6. Haji-Sheikh, A.: Flow Parameters on a Film Cooled Surface. Rep. No. ME-69-02(NSF Grant No. GK-1569), Univ. Texas (Arlington), [1969].

7. Sellers, John P.: Gaseous Film Cooling With Multiple Ejection Stations. AIAA J., vol. 1, no. 9, Sept. 1963, pp. 2154-2156.

8. Gooderum, Paul B.; Wood, George P.; and Brevoort, Maurice J.: Investigation With an Interferometer of the Turbulent Mixing of a Free Supersonic Jet. NACA Rep. 963, 1950. (Supersedes NACA TN 1857.)

9. Chapman, Dean R.; Kuehn, Donald M.; and Larson, Howard K.: Investigation of Separated Flows in Supersonic and Subsonic Streams With Emphasis on the Effect of Transition. NACA Rep. 1356, 1958. (Supersedes NACA TN 3869.)

10. Görtler, H.: Berechnung von Aufgaben der freien Turbulenz auf Grund eines neuen Näherungsansatzes. Z.F.a.M.M., Bd. 22, Nr. 5, Oct. 1942, pp. 244-254.

11. Reichardt, H.: Laws of Free Turbulence. R.T.P. Transl. No. 1752, Brit. Min. Aircraft Prod. (From V.D.I. Forschungsheft, No. 414, May/June 1942, pp. 1-22.)

12. Schlichting, Hermann (J. Kestin, transl.): Boundary-Layer Theory. Sixth ed., McGraw-Hill Book Co., Inc., 1968.

13. Tollmien, Walter: Calculation of Turbulent Expansion Processes. NACA TM 1085, 1945.

14. Korst, H. H.: A Theory for Base Pressures in Transonic and Supersonic Flow. J. Appl. Mech., vol. 23, 1956, pp. 593-600.

15. Chapman, Dean R.; Wimbrow, William R.; and Kester, Robert H.: Experimental Investigation of Base Pressure on Blunt-Trailing-Edge Wings at Supersonic Velocities. NACA Rep. 1109, 1952. (Supersedes NACA TN 2611.)

16. Crocco, Luigi; and Lees, Lester: A Mixing Theory for the Interaction Between Dissipative Flow and Nearly Isentropic Streams. J. Aeronaut. Sci., vol. 19, no. 10, Oct. 1952, pp. 649-676.

17. Van Driest, E. R.: Turbulent Boundary Layer in Compressive Fluids. J. Aeronaut. Sci., vol. 18, no. 3, Mar. 1951, pp. 145-160, 216.

18. Bogdonoff, S. M.; and Solarski, A. H.: A Preliminary Investigation of a Shock Wave – Turbulent Boundary Layer Interaction. Rep. No. 184 (Contract N6-ori-270, Task Order No. 6, Project Number NR 061-049), Aero. Eng. Lab., Nov. 30, 1951.

19. Schubauer, G. B.; and Klebanoff, P. S.: Investigation of Separation of the Turbulent Boundary Layer. NACA Rep. 1030, 1951. (Supersedes NACA TN 2133.)

20. Chapman, Dean R.: Laminar Mixing of a Compressible Fluid. NACA Rep. 958, 1950.

21. Chapman, Dean R.: A Theoretical Analysis of Heat Transfer in Regions of Separated Flow. NACA TN 3792, 1956.

NASA-Langley, 1970 —— 33 L-6689

01U 001 37 51 3DS 7C316 00903
AIR FORCE WEAPONS LABORATORY /WLOL/
KIRTLAND AFB, NEW MEXICO 87117

ATT E. LOU BOWMAN, CHIEF,TECH. LIBRARY

"The aeronautical and space activities of the United States shall be conducted so as to contribute . . . to the expansion of human knowledge of phenomena in the atmosphere and space. The Administration shall provide for the widest practicable and appropriate dissemination of information concerning its activities and the results thereof."

—NATIONAL AERONAUTICS AND SPACE ACT OF 1958

NASA SCIENTIFIC AND TECHNICAL PUBLICATIONS

TECHNICAL REPORTS: Scientific and technical information considered important, complete, and a lasting contribution to existing knowledge.

TECHNICAL NOTES: Information less broad in scope but nevertheless of importance as a contribution to existing knowledge.

TECHNICAL MEMORANDUMS: Information receiving limited distribution because of preliminary data, security classification, or other reasons.

CONTRACTOR REPORTS: Scientific and technical information generated under a NASA contract or grant and considered an important contribution to existing knowledge.

TECHNICAL TRANSLATIONS: Information published in a foreign language considered to merit NASA distribution in English.

SPECIAL PUBLICATIONS: Information derived from or of value to NASA activities. Publications include conference proceedings, monographs, data compilations, handbooks, sourcebooks, and special bibliographies.

TECHNOLOGY UTILIZATION PUBLICATIONS: Information on technology used by NASA that may be of particular interest in commercial and other non-aerospace applications. Publications include Tech Briefs, Technology Utilization Reports and Notes, and Technology Surveys.

Details on the availability of these publications may be obtained from:

SCIENTIFIC AND TECHNICAL INFORMATION DIVISION

NATIONAL AERONAUTICS AND SPACE ADMINISTRATION

Washington, D.C. 20546